IDA

INSTITUTE FOR DEFENSE ANALYSES

Analysis of Airborne Magnetometer Data from Tests at Aberdeen Proving Ground, Maryland, July 2002

Michael Tuley
Elvis Dieguez
John Biddle

July 2004

IDA Document D-3015
Log: H 04-001303

Report Documentation Page

Form Approved
OMB No. 0704-0188

1. REPORT DATE	2. REPORT TYPE	3. DATES COVERED
00 JUL 2004	**N/A**	**-**

4. TITLE AND SUBTITLE	5a. CONTRACT NUMBER
Analysis of Airborne Magnetometer Data from Tests at Aberdeen Proving Ground, Maryland, July 2002	5b. GRANT NUMBER
	5c. PROGRAM ELEMENT NUMBER
6. AUTHOR(S)	5d. PROJECT NUMBER
	5e. TASK NUMBER
	5f. WORK UNIT NUMBER
7. PERFORMING ORGANIZATION NAME(S) AND ADDRESS(ES) **Institute for Defense Analyses 4850 Mark Center Drive Alexandria, VA 22311-1882**	8. PERFORMING ORGANIZATION REPORT NUMBER
9. SPONSORING/MONITORING AGENCY NAME(S) AND ADDRESS(ES)	10. SPONSOR/MONITOR'S ACRONYM(S)
	11. SPONSOR/MONITOR'S REPORT NUMBER(S)

12. DISTRIBUTION/AVAILABILITY STATEMENT
Approved for public release, distribution unlimited

13. SUPPLEMENTARY NOTES
The original document contains color images.

14. ABSTRACT

15. SUBJECT TERMS

16. SECURITY CLASSIFICATION OF:			17. LIMITATION OF ABSTRACT	18. NUMBER OF PAGES	19a. NAME OF RESPONSIBLE PERSON
a. REPORT	b. ABSTRACT	c. THIS PAGE			
unclassified	**unclassified**	**unclassified**	**SAR**	**70**	

This work was conducted under contract DASW01 04 C 0003, Task AM-2-1528, for the Office of the Deputy Under Secretary of Defense for Science and Technology (DUSD(SERDP/ESTCP)). The publication of this IDA document does not indicate endorsement by the Department of Defense, nor should the contents be construed as reflecting the official position of that Agency.

INSTITUTE FOR DEFENSE ANALYSES

IDA Document D-3015

Analysis of Airborne Magnetometer Data from Tests at Aberdeen Proving Ground, Maryland, July 2002

Michael Tuley
Elvis Dieguez
John Biddle

PREFACE

This document was prepared under a task titled “ESTCP/SERDP: Assessment of Traditional and Emerging Approaches to the Detection and Identification of Surface and Buried Unexploded Ordnance.” The authors would like to thank Drs. Jeff Marqusee and Anne Andrews of the ESTCP/SERDP Program Office for their guidance in carrying out this analysis and for their careful review of the report. In addition, we would like to express our gratitude to the Oak Ridge National Laboratory and Naval Research Laboratory teams for their cooperation in this effort. Both groups’ willingness to answer questions concerning their systems, the way they were operated, and the data collected made the analysis job easier and more complete. Their reviews of the draft versions of the report raised excellent questions whose treatment in the final version have made this a better report.

CONTENTS

TABLES

FIGURES

EXECUTIVE SUMMARY

In July 2002, the Naval Research Laboratory (NRL) Airborne Multi-Sensor Towed Array Detection System (aMTADS) and the Oak Ridge National Laboratory Airborne Geophysics System (ORAGS) magnetometer systems surveyed several areas at the Aberdeen Proving Ground. Topographies and land cover ranged from flat and grassy, treed with brush, and wetlands to shallow ponds and marine offshore areas. The systems employed similar cesium-vapor, total-field magnetometers, but differed in platform setup and data processing:

- Both systems employ similar Bell helicopters and magnetometers mounted on booms. aMTADS mounts seven sensors on a forward boom. ORAGS deploys four sensors on a forward boom and four on a mid-ship boom.
- The two teams use different Global Positioning System (GPS)-based systems to provide location and attitude data and different altimeter combinations to provide height. Each team has developed its own algorithms for data calibration, smoothing, and interference reduction.
- The Oak Ridge system uses automatic target recognition algorithms to process the magnetometer data and classify targets. The NRL system relies on human judgment aided by computer-implemented, dipole-fit routines.

Probability of detection, background alarm rates, and other appropriate statistics were calculated for aMTADS and ORAGS through two major methodologies:

- 163 unexploded ordnance (UXO) items comprising 60 mm and 81 mm mortars and 105 mm and 155 mm shells were buried among intrinsic clutter at four topographically different sites.
- A dig list of unknown items was generated using data from both systems, and a subset of the unknown items was subsequently dug and identified.

Each system provided an ordered list of detections and assigned each detection a "confidence of ordnance" ranging from 1 being "high confidence UXO" to 6 being "high confidence clutter."

A priori consideration of the similarity between aMTADS and ORAGS suggests that they should perform about the same. However, their different platform setups, operating parameters (principally altitude and speed), and data-processing methods produced different results, with aMTADS performing better than ORAGS, particularly in

the more benign environments. Based on the results, we have drawn the following conclusions:

- If maximum sensitivity is desired, it is important that the system design allow very low-level flight in areas where that is possible. Careful attention to reducing apparent spatial background variations caused by platform dynamics effects is also crucial to obtaining maximum detection sensitivity. In the very benign airfield terrain and background, aMTADS detected 49 of 52 emplaced items including all three 60 mm mortars and eighteen of twenty-one 81 mm mortars, while ORAGS, flying about a meter higher and three times as fast and with four times the background standard deviation, detected 14 fewer emplaced items, missing 1 of the 60 mm, 11 of the 81 mm and 5 of the 105 mm.
- Successful detection of UXO targets in bodies of water will require knowledge of the burial depth and type of ordnance expected. Helicopter systems such as these already have the disadvantage of a sensor that is a meter or two above the surface. Because of the $1/(\text{distance})^3$ signal falloff, even moderate target depths make the detection of all but large targets marginal.
- Neither system shows significant individual target detection capability in highly cluttered areas.
- Target location accuracy is important for unambiguous target recovery. aMTADS demonstrates that average radial position errors of less than 40 cm are possible from an airborne system using real-time, differential GPS. However, obtaining that degree of accuracy requires reliable sensing and precise accounting for helicopter dynamic effects on sensor position.
- Accurate automatic detection and classification algorithms would be of significant benefit for systems (such as the ones demonstrated here) that are capable of surveying hundreds of acres per day. Current automatic algorithms, however, do not perform as reliably as human analysts. Particularly in the detection phase, they result in many more anomalies that would have to be dug, without adequate discrimination capability to make up for the additional detections.
- Current-generation helicopter-borne magnetometer systems are capable of reliably detecting areas of high ferrous clutter/UXO density. It appears they are not suitable for general survey use to detect individual ordnance items, except in special conditions that provide a combination of benign terrain, low background clutter, and appropriate UXO sizes (>60 mm). Even then, lower and slower flight than indicated in system specifications will likely be required to achieve adequate detection performance.

I. INTRODUCTION

The purpose of this technical report is to provide results of IDA's evaluation of data collected by the Naval Research Laboratory (NRL) and the Oak Ridge National Laboratory (ORNL) airborne magnetometer systems in testing conducted at Aberdeen Proving Ground (APG), Maryland, during July 2002. We first give a brief description of the test areas and the data collected. We then summarize the detailed analysis to allow the reader to understand the basis upon which conclusions are drawn. ORNL and NRL report on this operation in references 1 and 2. Those documents provide more detail on the helicopter-mounted systems and on the detection and classification processing. Reference 3, the U.S. Army Aberdeen Test Center report on the surveys, provides additional detail on the demonstration areas and on the emplacement and removal of the seeded ordnance items.

A. APG TEST SITES [3, 4]

The Aberdeen testing took advantage of some areas within the proving ground that contain preexisting ordnance items and scrap, as well as several areas that were seeded with ordnance from the Standardized Test Site inventory. A calibration area was established near an on-base airfield historically clear of UXO, and 10 ordnance items whose locations and orientations were known to the demonstrators were buried in an area thought to be relatively uncluttered. Although the calibration area generally had little clutter, a very large magnetic anomaly in the vicinity of several of the calibration targets negated their usefulness for analysis. In addition, an open field area in the vicinity of the airfield was seeded with 52 ordnance items in locations unknown to the demonstrators. Figure 1 is an aerial photograph of the airfield, with the calibration (checkout) and open field areas shown.

The remaining areas with seeded ordnance were a dewatering pond area (47 items); an active recovery field for indirect-fire weapons (24 items), which also contained areas of phragmites (8 items); and littoral areas (32 items). Surveys were also conducted over a mine, grenade, and direct-fire weapon range and over a Chesapeake Bay tidal water area that is an old impact area. In those areas, no ordnance was emplaced or dug, and no scoring was done due to the high density of UXO. More detail concerning the individual sites is provided in the analysis section.

Figure 1. Airfield Area with the Calibration (Checkout) and Open Field Areas Marked

B. SENSOR PLATFORMS [5, 6]

Two helicopter-borne sensor arrays were demonstrated in the tests at APG. Each is carried on a similar Bell 206L Long Ranger helicopter. The arrays employ a cesium vapor, total field magnetometer (Geometrics Model 822 variants) array mounted on a nonmetallic boom, and a differential Global Positioning System (GPS) to provide accurate position data for anomaly location and for discrimination algorithm inversion. The arrays and navigation instrumentation, however, differ in a number of details.

The Oak Ridge Airborne Geophysics System (ORAGS), developed by ORNL and shown in Figure 2, deploys the magnetometer sensors on an "Arrowhead" array. This array includes four outboard magnetometers, two on each side of the aircraft, mounted on an amidships horizontal boom, and four magnetometers spaced horizontally on a boom forward of the helicopter nose. Horizontal spacing of the magnetometers is 1.75 m. Although this arrangement provides a very wide array, in flight the pilot is generally unable to see the wide amidships booms, and the fore-aft spacing complicates signal leveling among the sensors. The ORAGS data-collection system samples at a 1,200 Hz rate, but commonly downsamples to 120 Hz for analysis. The data provided to IDA were at the 120 Hz rate.

Figure 2. Oak Ridge Airborne Geophysics System

The airborne version of the NRL Multi-Sensor Towed Array Detection System (MTADS) shown in Figure 3, which we designate airborne Multi-Sensor Towed Array Detection System (aMTADS), is an outgrowth of an earlier vehicle-towed system. It employs seven magnetometers on a single horizontal boom in front of the helicopter nose. Magnetometer spacing is 1.5 m, and sensor sampling is done at 100 Hz.

Figure 3. NRL Airborne Multi-Sensor Towed Array Detection System

Specifications for both systems call for an altitude of a few meters above the ground and a speed of around 20 m/s. Operation at the nominal speed results in down-track sample spacings of 15–20 cm for the two systems, which is much finer than the

cross-track sampling. Cross-track sampling finer than the 1.5 m or 1.75 m sensor spacing can be provided by multiple or overlapping passes at the expense of area coverage rate. For example, aMTADS, with its 9 m array width, typically flies 7.0 m line separations (the design specification calls for 7.5 m line separations). In addition, in the airfield area, aMTADS speeds were generally around 5 m/s and altitudes were closer to 1 m. ORAGS speed and altitude for those measurements were closer to 15 m/s and 2 m. Effects caused by differences in altitude and speed are discussed where they affect analyzed results.

C. DATA ANALYZED

The demonstrators provided two types of data to IDA for analysis: magnetometer data and target-detection lists. Raw and processed magnetometer data were provided for a high-altitude flight segment and for both the airfield sites. Detection lists were provided by both demonstrators for the three sites containing seeded ordnance. ORNL provided two lists. One employs what they term a univariate detection and discrimination algorithm and the other a multivariate algorithm. The two lists were scored independently for both detection/discrimination performance and location-error statistics. These lists included NAD83 coordinates; target size, moment, inclination, and azimuth; and a number indicating UXO likelihood. The standard classification system specified by the Environmental Security Technology Certification Program (ESTCP) sorts detections into six categories from 1 to 6, with 1 denoting most likely UXO and 6 denoting most likely clutter. That target-classification hierarchy was used to establish receiver operating characteristic (ROC) curves for each system.

II. ANALYSIS

A. OVERVIEW

Two basic types of analysis were undertaken using the APG data. The first was an instrument sensitivity analysis that utilized high-altitude magnetometer data and data collected over the airfield calibration and open field areas. Sensor noise floors were established for the high-altitude case, where only internal noise and platform effects should be evident. Noise was also calculated for low-altitude operation, where small-scale clutter was expected to raise the noise floor. Peak signal response was determined over a number of targets to assess typical signal-to-noise ratios (SNRs) for various target types. Detection statistics were based on the emplaced ordnance in the airfield open field area, the dewatering ponds, and the active recovery field areas. Analysis is described and results are presented below for each of the measures of system performance examined. Note that ROC curves presented are in terms of probability of detection (Pd) of emplaced items versus the background alarm rate. Without full excavation of all anomalies, true ROC curves of Pd versus false-alarm probability or false-alarm rate cannot be generated. For the airfield open field area, subsequent examination of 20 anomalies from the operators' detection lists found 18 items to be non-ordnance-related clutter (mower blade, scrap iron, welding rods, etc.). Two items, found together, were inert volcano mines. Thus, for the airfield, which was historically clear of UXO, the limited excavations appear to indicate that the background alarms are heavily dominated by non-ordnance-related clutter. That is not the case for the other areas.

B. SENSITIVITY

The goal of the sensitivity analysis was to assess the noise properties of the two sensor arrays and to establish the SNR levels that could be achieved against a variety of targets. Ultimately, SNR is a function of a number of system- and operation-related factors. These include the inherent sensitivity and internal noise characteristics of the cesium vapor magnetometers and data-collection system electronics, the ability of data processing to remove platform noise and large-scale geologic noise without suppressing signal components, the height of the sensor above the target, and the proximity of the peak data point to the actual peak of the magnetic response. While we made an attempt to understand the factors affecting relative sensor capabilities, the focus of this effort was to

assess performance based on the data delivered by the demonstrators. Because the processed data were used to make detection and classification decisions, the emphasis was on an analysis of those data; however, raw magnetometer data gathered in high-altitude flights were also analyzed to understand the noise added by the platforms.

The first analysis undertaken utilized raw and processed magnetometer data from the high-altitude flights to establish a fundamental noise floor for each of the sensor systems. Figure 4 provides the output of a fast Fourier transform (FFT) of raw, de-medianed, high-altitude data from both sensors. The composite spectrum was produced by taking an FFT of 20 sec of each magnetometer time series and then summing the spectral magnitudes. The data are displayed in decibel space to allow the data dynamic range to be better visualized, and each abscissa is scaled to the highest unambiguous frequency provided by the sample rate (60 Hz for ORAGS and 50 Hz for aMTADS). No attempt was made to normalize the response between the two systems, so the absolute levels on the two plots are meaningless. On both plots, the strong signal near 6.5 Hz and its harmonics are due to the helicopter blades. Most of the target information lies at frequencies well below the blade modulation signals, and one major purpose of data preprocessing is to remove the high-frequency platform interference without removing the target signal.

Figure 5 provides the ORNL data record from which the ORAGS spectrum above was produced. The upper figure provides the time history of each of the magnetometers, and the bottom figure plots the same data after a de-median filter has been applied. Only the 20-second segment between 15 and 35 seconds was used in the subsequent analysis, not only because it visually represents a relatively constant segment of the data, but because it also contains enough points to provide good statistics. Figure 6 provides histograms of the raw, de-medianed, high-altitude data from that segment and the same data after ORNL processing. Note that processing, which basically applies filtering to remove high-frequency components, significantly reduces data spread. For the high-altitude data, the noise signal is nominally Gaussian, as expected, and has a standard deviation of 0.56 nT. Processing reduces the standard deviation to 0.14 nT.

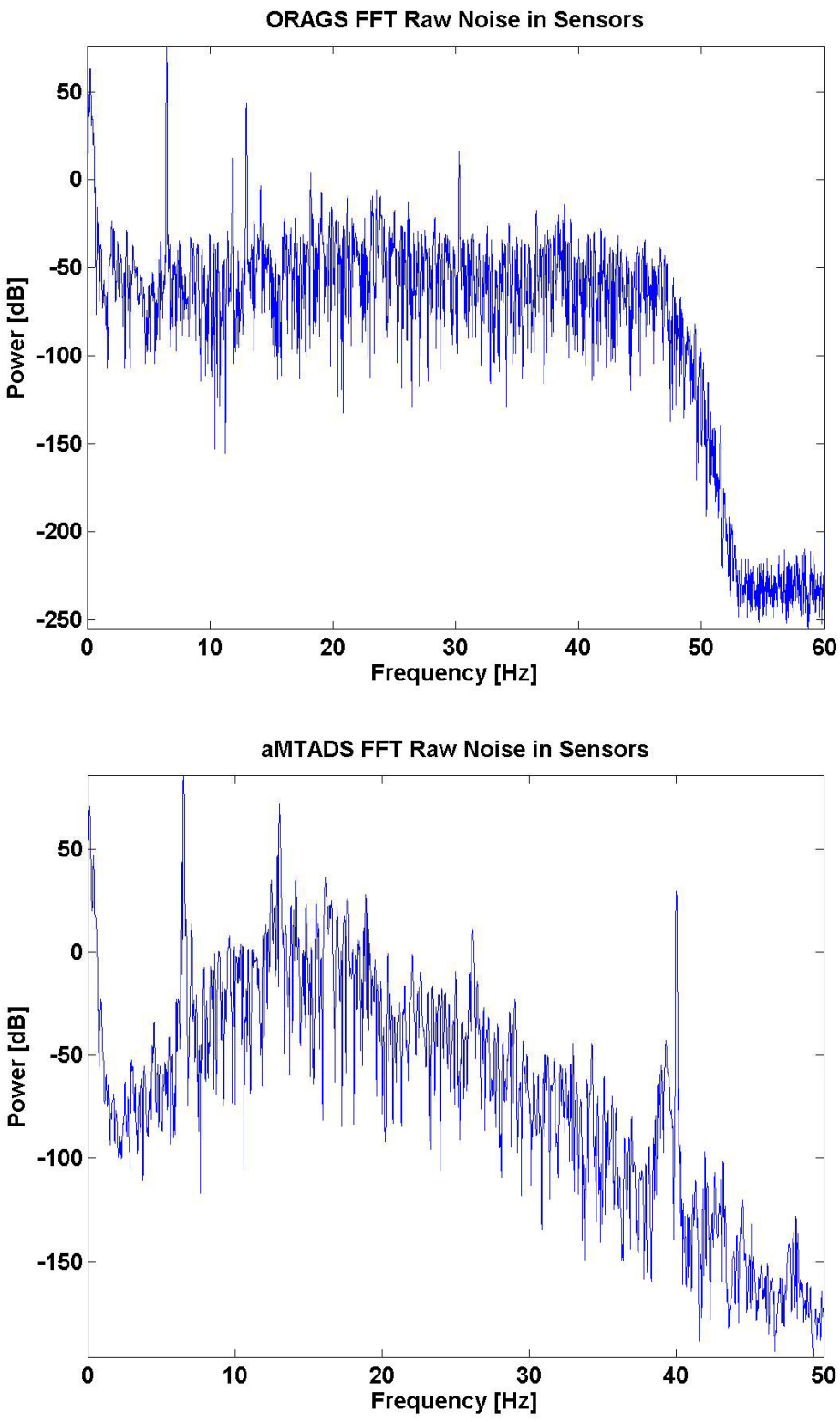

Figure 4. Sensor Spectral Output from Raw, High-Altitude Data

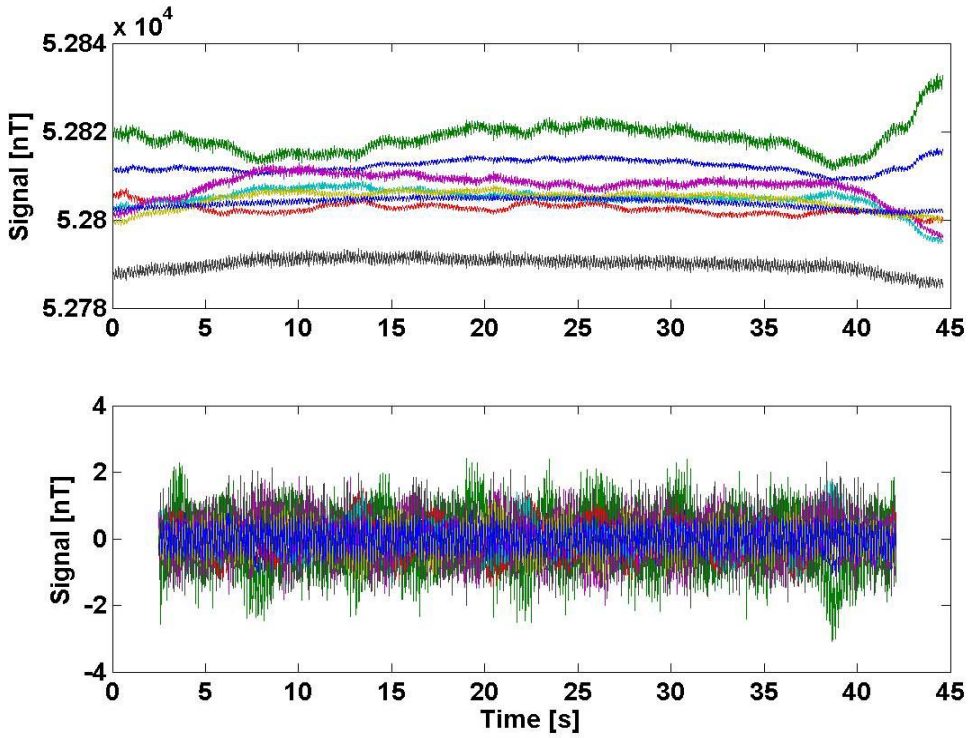

Figure 5. Oak Ridge Airborne Geophysics System High-Altitude Raw Data and After Passage through a De-median Filter

Figure 7 provides approximate altitude (height above ellipsoid, HAE) and signal data for the aMTADS system, where output from each of the magnetometer sensors is plotted. Note that only six magnetometer signals are provided in the plots. Because one magnetometer was not functioning correctly during the high-altitude calibrations, its signal was not used in the high-altitude noise analysis. The HAE data are included because NRL chose to fly a relatively complex high-altitude pattern that included course changes and maneuvers. The maneuvers are evident in the HAE data after 622 seconds, which show different sensor altitudes due to helicopter banking. To provide a representative sample for straight flight, only the raw data from 600 to 620 seconds were used in the analysis. The raw data contain a long-term trend and some differences between the individual sensor channels. As with the ORAGS data, IDA removed these by applying a de-median filter to each channel. Figure 8 provides a histogram of the raw high-altitude magnetometer data after the de-median operation and after NRL signal processing. The noise signal is nominally Gaussian, as expected, and has a standard deviation of 1.36 nT.

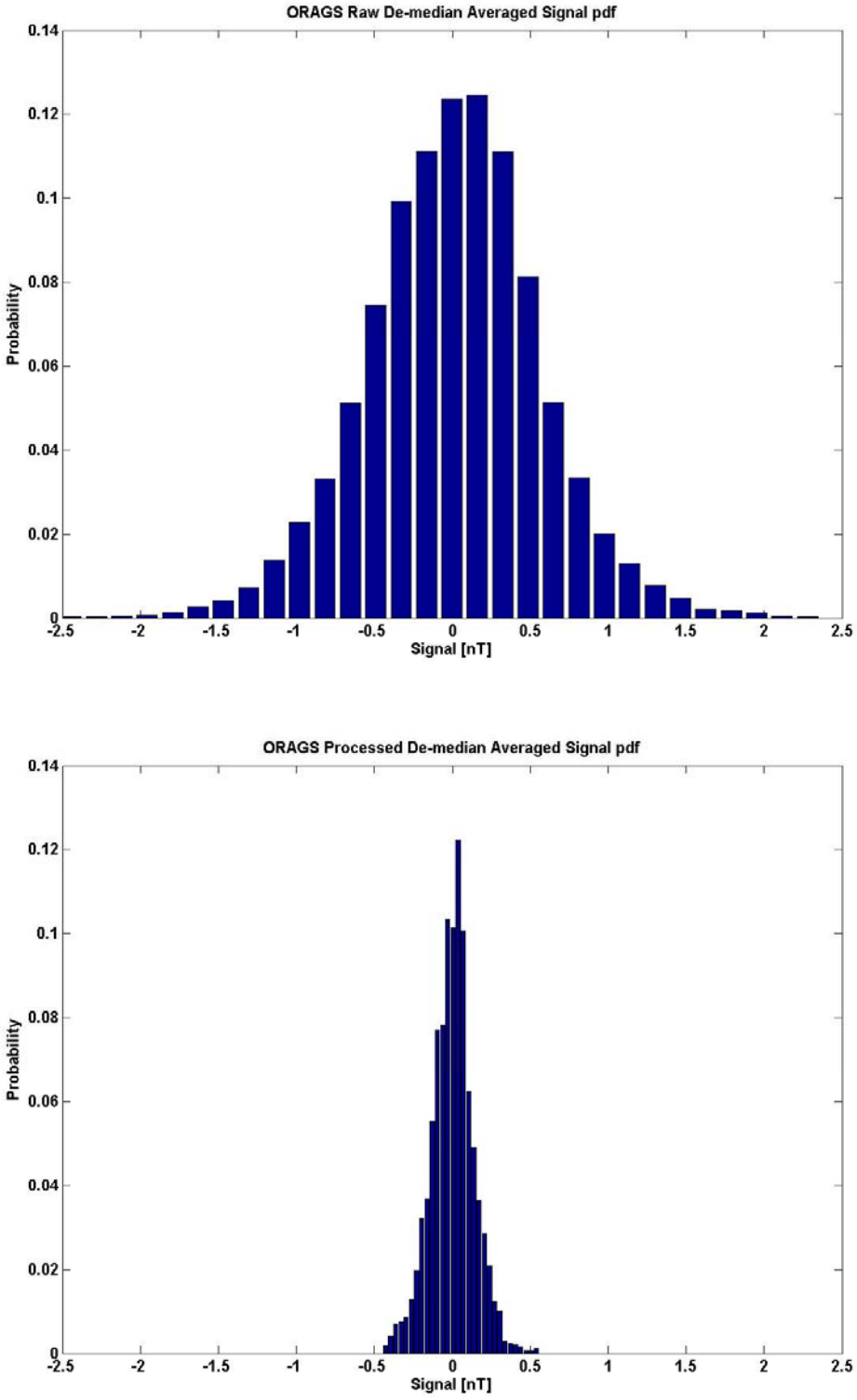

Figure 6. Histograms of Oak Ridge Airborne Geophysics System High-Altitude De-medianed Data and Processed Data

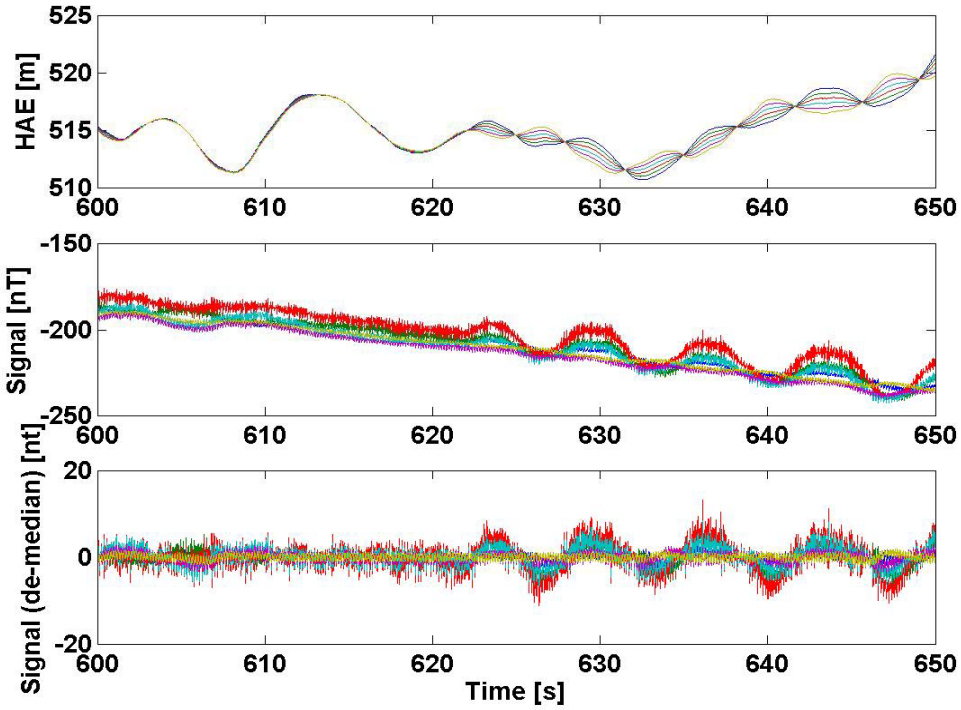

Figure 7. Raw High-Altitude Data from Airborne Multi-Sensor Towed Array Detection System

The processed high-altitude data histogram in Figure 8 provides a standard deviation of 0.5 nT. Subsequent analysis of quiet areas in the airfield calibration and open field areas yielded aMTADS standard deviation values as low as 0.09 nT. Other than effects of aircraft maneuvers and speed, there is no physical reason the high-altitude data should be noisier than near-ground data, so we investigated the spectrum for the processed high-altitude data. Residual energy in the 6.5 Hz region was clearly visible in the spectrum, indicating that the preprocessing used for the high-altitude data had not removed all the blade noise. In its standard processing, NRL applies both a notch filter and a low-pass filter to the raw data [2]. We crudely simulated the effects of low-pass filtering by zeroing the FFT spectral bins above 6.45 Hz and inverse transforming the complex spectral data to recover a time series. After the crude low-pass filtering operation, the aMTADS processed data achieve a 0.16 nT standard deviation, almost equal to that seen with ORAGS. Although this value is still larger than seen in some of the near-ground quiet areas, we attribute the difference to our crude filtering scheme. Note that the high-altitude noise data were not used in any subsequent signal-to-noise ratio analysis. For those analyses, the low-altitude noise in the local area is a more realistic measure of system performance. The high-altitude noise analysis was simply

done as a sanity check and to ensure that we understood the data provided to IDA. All the scoring analysis used the processed data as it was delivered by the two demonstrators.

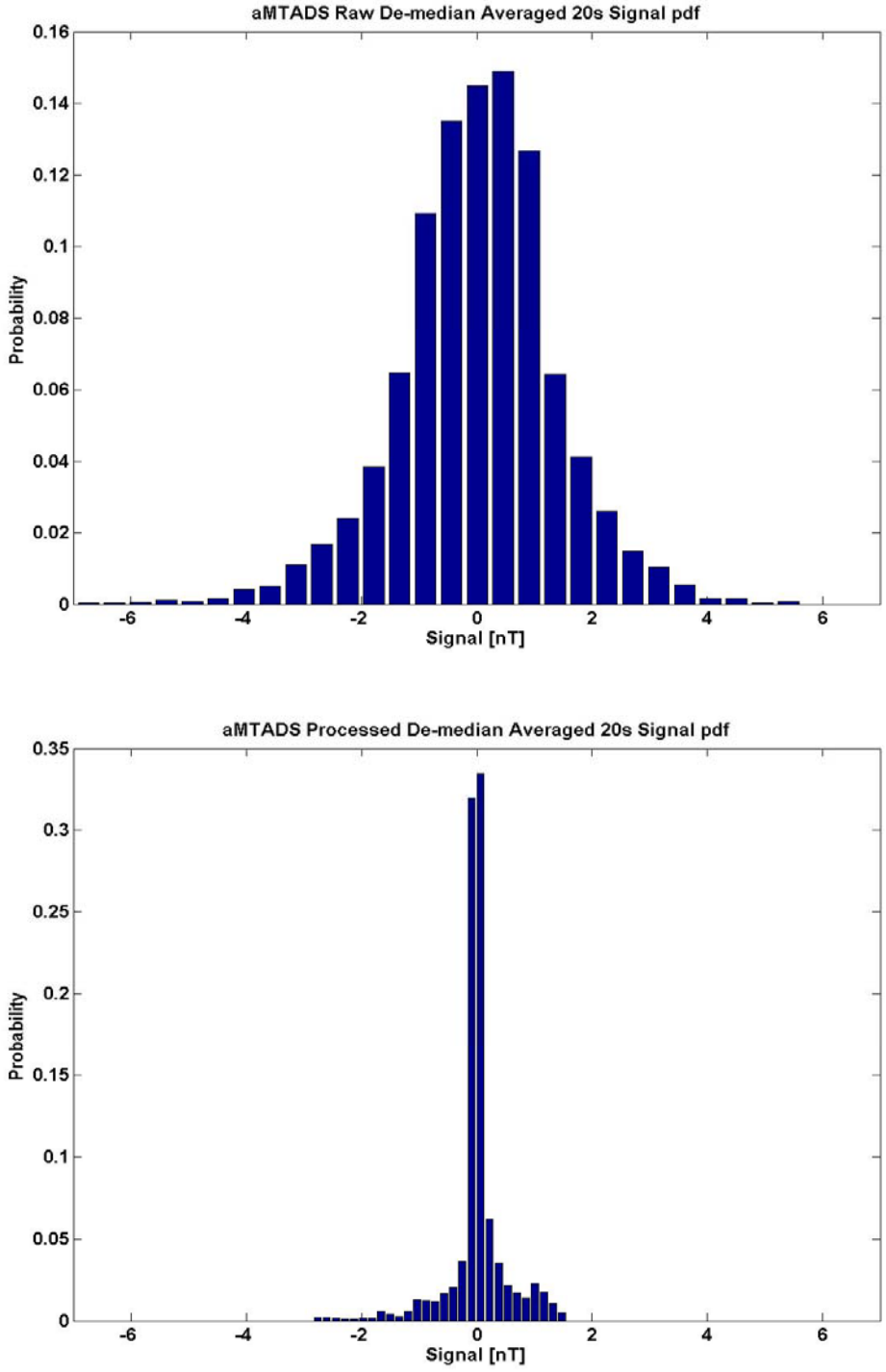

Figure 8. Histograms of Airborne Multi-Sensor Towed Array Detection System High-Altitude De-medianed Data and Processed Data

Having established the noise floors for the sensors, the remaining question to be answered regarding sensitivity was what target signal could be achieved over various targets and thereby what SNR. Because it was likely that noise performance would degrade close to the ground, where small ferrous clutter items and fine-scale geology could raise the noise floor, the noise used to reference SNR was that from a visually quiet area in the vicinity of the targets.

The first area assessed for SNR performance was the calibration lane area within the airfield. That area contained two each of five ordnance types, all horizontal, with one buried facing north-south and one east-west. Figure 9 shows ORAGS and aMTADS magnetometer maps of the calibration area. Target locations are indicated by an × for the 60 mm, and going from northwest to southeast, the remaining targets in pairs denoted by circles of different colors are 2.75 inch, 81 mm, 105 mm, and 155 mm. Data from the box at the top of the area were used to establish the noise floor for each system.

Note that both figures contain a bright anomaly centered at approximately –100 N and –50 E. That anomaly prevented analysis of the east-most 81 mm target. In addition, no peak could be chosen in the ORAGS data for the one of the two 60 mm mortar targets or in either data set for one of the 2.75-inch rounds. Table 1 provides peak magnetometer levels from the data for each of the targets that could be analyzed. Two columns of peak values are provided for each system. In each case the left column is for the more northwesterly item of each ordnance pair in Figure 9, and the right column is for the more southeasterly item.

Individual peak signatures for a given ordnance type can vary significantly because of ordnance orientation and also because of possible offsets (with 1.5 m or 1.75 m cross-range sensor spacing) of the nearest magnetometer from the signal's actual peak. Nevertheless, a reasonable sample of items should be expected to average the offset potential among the sensors, and in any event, the SNR achieved is one legitimate measure of how a system actually performed. In this case, if only common ordnance items are considered, the average peak signal seen by aMTADS is 1.8 times larger than the peak signal seen by ORAGS.

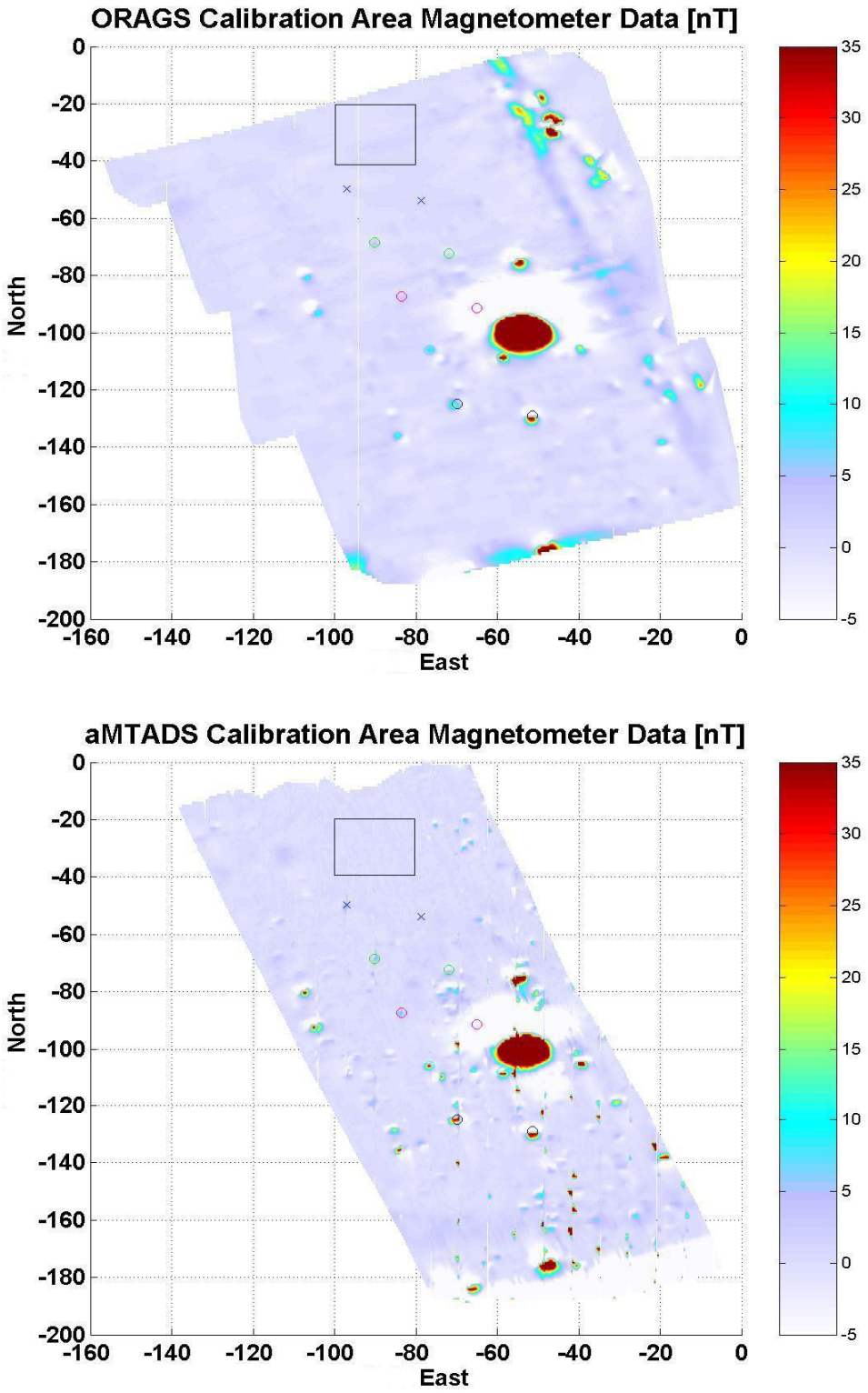

Figure 9. Oak Ridge Airborne Geophysics System and Airborne Multi-Sensor Towed Array Detection System Magnetometer Data for the Airfield Calibration Area

Table 1. Magnetometer Peaks from the Airfield Calibration Area

Target Pair Type	ORAGS Peak (nT)		aMTADS Peak (nT)	
60 mm	2.44	--	8.78	3.82
2.75 inch	5.60	--	9.84	--
81 mm	3.89	--	11.32	--
105 mm	11.93	55.79	41.69	49.75
155 mm	19.23	43.65	56.51	85.17

To convert peak signal to peak SNR, the quiet area in the box was analyzed to establish a background noise level for each system. Figure 10 provides blow-ups of the quiet area for each system, with scales chosen to emphasize small variations in signal. In Figure 10, the ORAGS return shows a pattern on a scale unlikely to be connected with small clutter anomalies, while the aMTADS return is much more constant, with the exception of what may be a small anomaly in the northwest corner. Figure 11 shows the processed data histograms over that area, where the difference in noise characteristics is even more obvious. The aMTADS system shows a noise distribution that is approximately Gaussian, albeit with some asymmetry, and a standard deviation of 0.09 nT. ORAGS, on the other hand, shows a decidedly non-Gaussian histogram. The processed data that IDA analyzed were provided in a map format (i.e., a data array that gave only signal amplitude and position) and not keyed to the particular sensor in the array that collected the data. Part of the manipulation to transform raw magnetometer data into processed data is to level the sensor outputs. The map of the quiet area and the shape of the ORAGS histogram imply that leveling was not perfect, and the density function appears to be the result of summing several non-zero-mean Gaussians. Because of that, the noise standard deviation in the quiet area for ORAGS was 0.51 nT.

Using the background noise measured for each sensor array and the peaks of Table 1, SNR values were calculated for the ordnance items analyzed. Those values are shown in Table 2. The combination of the lower sensor noise level and the larger signal gives the aMTADS about a factor of 10 advantage in peak SNR level on comparable targets.

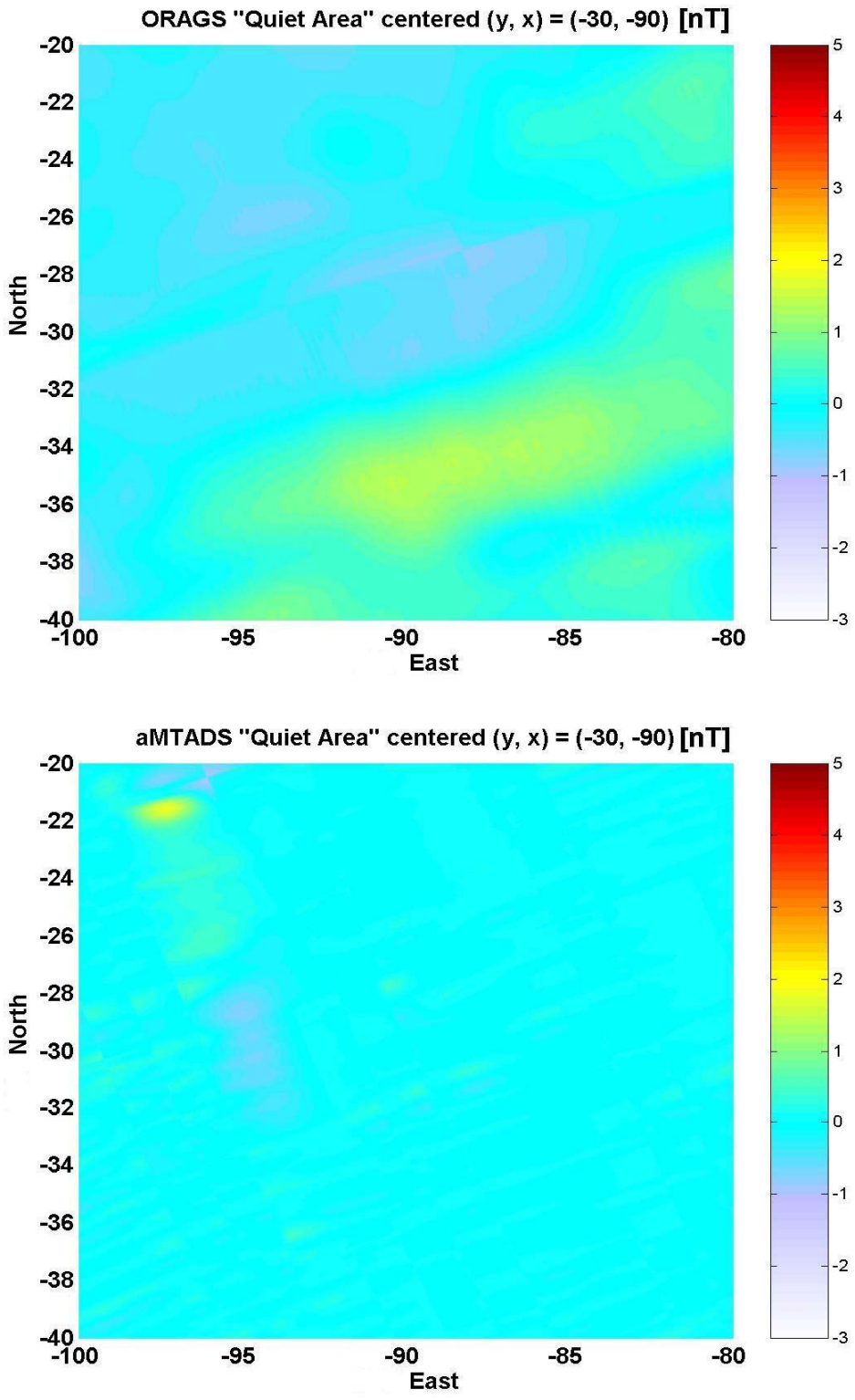

Figure 10. Magnetometer Maps for the Airfield Calibration Lane Quiet Area

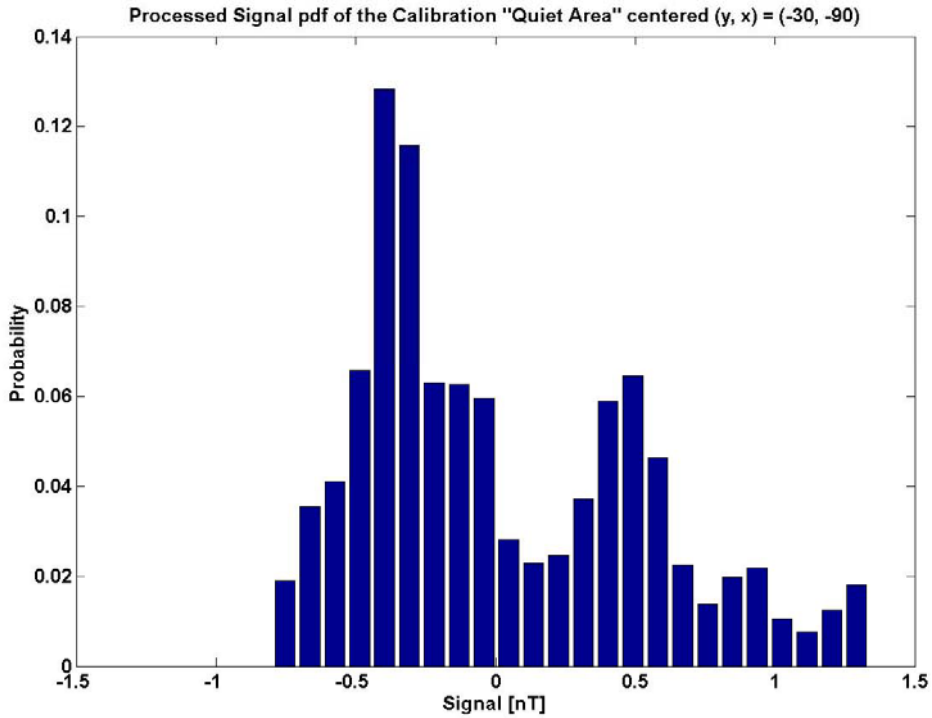

(a) ORAGS

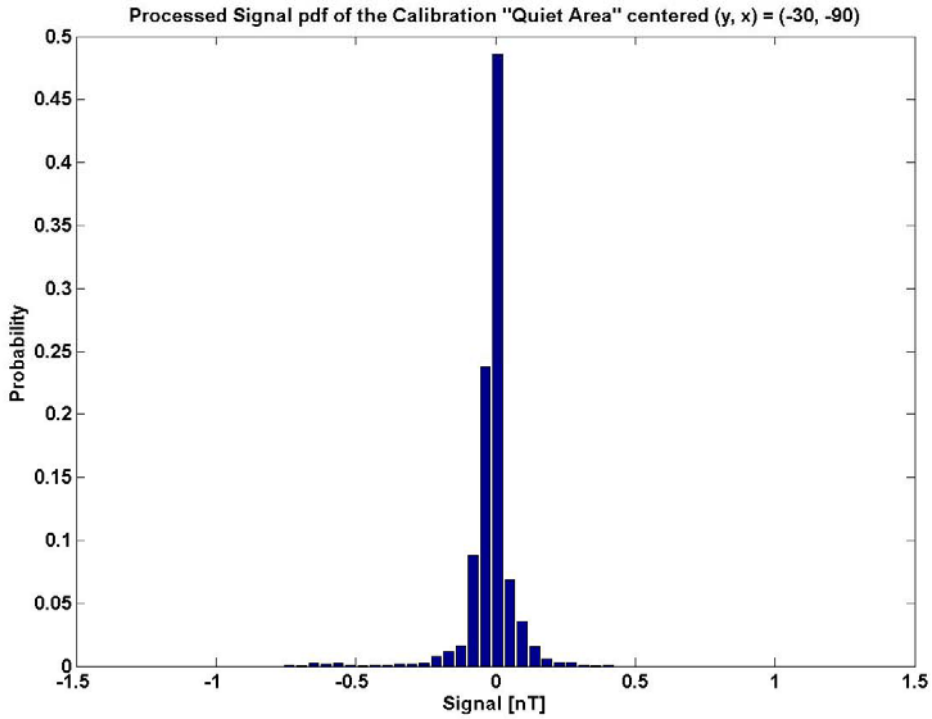

(b) aMTADS

Figure 11. Histograms of the Magnetometer Outputs for the Airfield Calibration Lane Quiet Area for (a) ORAGS and (b) aMTADS

Table 2. Peak SNR Values from the Airfield Calibration Area

Target Pair Type	ORAGS SNR		aMTADS SNR	
60 mm	4.8	--	97.6	42.4
2.75 inch	11.0	--	109.3	--
81 mm	7.6	--	125.8	--
105 mm	23.4	109.4	463.2	552.8
155 mm	37.7	85.6	627.9	946.3

We felt some concern limiting the SNR analysis to the calibration area, particularly because much of the SNR difference was a result of a lower noise background for the aMTADS. Therefore, additional SNR analysis was accomplished on selected targets in the airfield open field area. Figure 12 provides magnetometer maps for the ORAGS and aMTADS collections at that site, with the six items chosen for further SNR analysis denoted by arrows and numbers. The criteria used for choosing the items were that they show a clear peak in both data sets and that they lie in an area where there appears to be no contamination of the target signal by other anomalies. No 60 mm targets were chosen. Table 3 provides the signal levels for the 6 targets analyzed.

Table 3. Magnetometer Peaks from the Airfield Open Field Area

Target #	Target Type	ORAGS (nT)	aMTADS (nT)	aMTADS/ORAGS
1	105 mm	32.33	172.86	5.35
2	105 mm	33.60	123.16	3.67
3	105 mm	8.20	31.99	3.90
4	81 mm	4.79	24.21	5.05
5	81 mm	6.74	24.77	3.68
6	81 mm	5.61	5.73	1.02

With the exception of one 81 mm mortar, the peak aMTADS signals were three to five times those of the ORAGS system. A potential reason for the higher aMTADS signal levels is the higher data density provided by that system in this survey. In one airfield area analyzed, the ORAGS data provided about 4 points/m^2. This is slightly denser than the 3.4 points/m^2 that would be calculated for the array spacing and sample rate. In contrast, aMTADS provided 21 points/m^2, significantly more than the 3.3 points/m^2 that would be calculated for its sensor spacing and sample rate. Further investigation and discussions with the NRL team showed that the higher density was partially a result of the normal 7.0 m line spacing but mostly due to reduced helicopter speed.

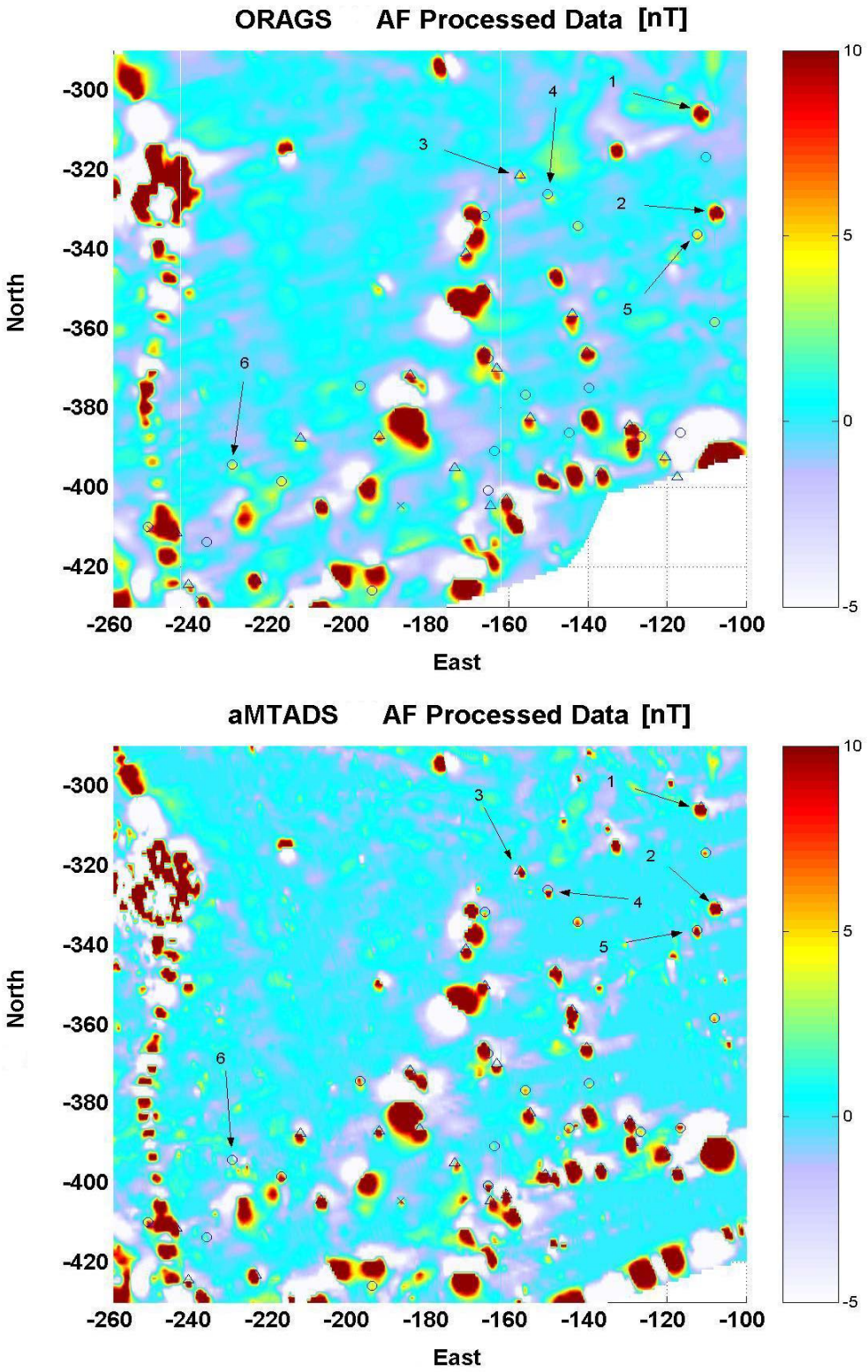

Figure 12. Oak Ridge Airborne Geophysics System and Airborne Multi-Sensor Towed Array Detection System Magnetometer Maps of the Airfield Open Field Area (Emplaced items are indicated by Δ for 105 mm, o for 81 mm, and × for 60 mm)

Increased data point density implies decreased point spacing down-range, cross-range, or both. In this case, the 7.0 m line spacing provides potentially decreased cross-range data spacing (if the sensor paths do not align in the overlap region, which in general they did not), and the slower speed provides decreased down-range spacing. Even at normal helicopter speed, the cross-range and down-range point separations are so different (1.5–1.75 m in cross-range vs. 0.15-0.2 m in down-range) that the potential benefits of decreasing each are different.

The major potential benefit of decreased cross-range spacing is increased probability that a data point will lie on the peak of the target return. For a helicopter at a 2 m altitude, a point target at the surface, and an assumed $1/(\text{distance})^3$ signal falloff, the peak signal provided by a target directly under an ORAGS sensor would be 1.3 times stronger than one with maximum separation from the sensor. For a 1 m helicopter altitude, the improvement is a factor of 2.3. For extended targets, however, the effect would be decreased. Thus, cross-range sample density can be only a part of the reason for the stronger aMTADS signal.

Because the spatial signal is significantly oversampled in the down-range direction, even at normal helicopter speeds, the advantages of closer sample spacing in that dimension are more subtle. Nevertheless, an advantage does arise because of the relationship between the spatial frequencies in which the target information lies and the temporal frequencies of the major interference source, the helicopter blade rate and its harmonics. With the aMTADS 100 Hz sample rate (50 Hz Nyquist fequency), the 6.5 Hz blade rate interference will always appear in a Doppler bin that is 13% of the total unaliased frequency band from the zero Doppler bin. In contrast, decreasing the down-range sample spacing increases the maximum unambiguous spatial frequency in proportion to the decreased spacing. Thus, the blade interference appears at an apparently higher spatial frequency for decreased sample spacing, and filtering to reduce that interference can be more effective with less effect on the spatial frequencies that provide target information. Because the benefits would strongly depend on the level of the blade interference, the details of the filtering used to suppress it, and the spatial frequencies of the target data, we have not attempted a quantitative analysis of performance improvement given by reduced down-range sample spacing. While it is unlikely a major effect, we point it out as an advantage of slower speed operation.

Although point spacing can certainly have some effect on relative signal strengths, helicopter altitude has a major effect because of the $1/(\text{distance})^3$ signal falloff. In the table below are estimates for the parameters of the dipoles for five of the six NRL

and ORNL targets from the airfield open field area analyzed in Table 3. (The sixth target was not analyzed because of its small peak amplitude for both systems.) To obtain these estimates, the NRL and ORNL processed data were interpolated to 25 cm resolution, a Matlab image was constructed using the interpolated data, a polygonal region was selected in the image to isolate a dipole, and this region was input to AETC Inc.'s dipole-fitting routine. The routine requires estimates of the background field, so we used an online resource, http://nssdc.gsfc.nasa.gov/space/model/models/igrf.html, to provide data for the magnitude and direction of the sea-level, background magnetic field at Aberdeen, Maryland. Tables 4 and 5 provide the location estimates from the dipole-fit routine and the ground truth values for the five targets analyzed. For both sets of data, the background magnetic field input was B_T = 52697.5 nT, Inclination = 58.5°, Declination = 3.6°. To assess the sensitivity of the results to the background field, we estimated target parameters with a different background (Pecos, Texas). While the estimated inclination and declination of the target changed, the position and depth estimates did not change significantly.

Table 4. Ground-Truth and Dipole Parameter Estimates Obtained from NRL Processed Data Using Background Field for Aberdeen, Maryland, at Sea Level

ID	Dipole Parameter Estimates			Truth		
	X	Y	Z	East	North	Depth
105MM-2	–111.28	–305.47	1.39	–111.30	–305.39	0.46
105MM-4	–107.36	–330.76	1.55	–107.36	–330.51	0.46
105MM-14	–156.95	–321.84	1.23	–157.28	–321.36	0.46
81MM-10	–149.77	–326.65	1.22	–150.08	–326.23	0.11
81MM-8	–112.34	–336.89	1.53	–112.31	–336.30	0.11

Table 5. Ground-Truth and Dipole Parameter Estimates Obtained from ORNL Processed Data Using Background Field for Aberdeen, Maryland, at Sea Level

ID	Dipole Parameter Estimates			Truth		
	X	Y	Z	East	North	Depth
105MM-2	–111.03	–305.79	2.55	–111.30	–305.39	0.46
105MM-4	–107.06	–331.11	2.34	–107.36	–330.51	0.46
105MM-14	–157.24	–321.87	1.86	–157.28	–321.36	0.46
81MM-10	–149.40	–326.72	1.93	–150.08	–326.23	0.11
81MM-8	–111.54	–336.98	2.14	–112.31	–336.30	0.11

The Z estimate from the dipole-fit routine is distance from the sensor to the target. From the ground truth, we know target depth and can estimate helicopter altitude, assuming that a sensor flew directly over the target. Table 6 provides an estimate of the helicopter altitude for each target, along with the factor by which the two signal amplitudes should differ for a 1/(distance)^3 relationship. The averages of the estimated signal ratios and the measured signal ratios differ by less than 10%. Thus, it appears that the major portion of the difference in signal can be explained by the difference in operating altitude. It is not surprising that basic system signal sensitivities should be very similar, as they are using the same cesium vapor magnetometer and there is no reason differences in electronics should markedly affect the signal amplitude.

Table 6. Estimated Helicopter Altitudes and Signal Differences Based on a (distance)$^{-3}$ Signal Amplitude Model

ID	aMTADS alt. estimate (m)	ORAGS alt. estimate (m)	Estimated signal ratio	Measured signal ratio
105MM-2	0.93	2.09	6.17	5.35
105MM-4	1.09	1.88	3.44	3.67
105MM-14	0.77	1.40	3.46	3.90
81MM-10	1.11	1.82	3.96	5.05
81MM-8	1.42	2.03	2.74	3.68
Average	1.06	1.84	3.95	4.33

Because of the lack of terrain relief or cover in the airfield area, both aircraft averaged altitudes lower than the nominal 2 m called out in the specifications. aMTADS took advantage of the very flat terrain to fly about a meter off the ground. If such low altitudes can be safely flown, and geology and clutter are benign, these data show that targets as small as 60 mm can be detected. However, the very rapid fall-off of signal with distance means that small increases in altitude are likely to significantly reduce detection capabilities for small targets.

Because signal is only one part of SNR, analysis of the noise levels for the two systems in the open field area was also required. The selection of a quiet area in the airfield open field area was not as straightforward as in the calibration area because of obvious small clutter peaks over much of the open field survey area. A tradeoff must be made between a sufficient number of points to provide good statistics and an area small enough to exclude unwanted anomalies. To assess noise level, several apparently quiet areas were chosen, then all points within an increasing radius of the center point were included in the noise calculation. In general, this provided a relatively stable noise standard deviation until an anomaly was reached that rapidly increased the value of the

standard deviation. Figure 13 shows blow-ups of maps produced by each system for one of the quiet areas chosen. Visually, this appears to be the quietest portion of the airfield open field area for both systems; other areas provided higher noise standard deviations for the systems that were obviously affected by local, small anomalies.

Figure 14 provides curves for the signal standard deviation as a function of radial distance from the reference point for both systems. As the radius increases, all points lying within the enclosing circle are used to calculate the noise standard deviation. In this case, ORAGS shows a monotonic increase in standard deviation vs. radius until in the vicinity of the small anomaly around 17 m. This behavior may be symptomatic of offsets across the array. On the other hand, aMTADS shows a low but relatively stable noise floor that increases only as an obvious anomaly is reached.

Using the best case results for ORAGS, those for the 5 m radius circle, the noise standard deviation for ORAGS is 0.36 nT and for aMTADS is 0.09 nT. Based on those values and the peak signals of Table 3, Table 7 gives SNR values for the targets in the airfield open field area.

These results are, in general, consistent with those of the airfield calibration area. That is, the aMTADS provides a noise floor that is lower and peak signals that are higher than the ORAGS, resulting in an SNR difference of nearly a factor of 17. These apparent sensitivity differences are reflected in the detection performance described in the next section.

C. DETECTION

The detection analysis for APG focused on assessing the percentage of emplaced ordnance items detected in each of the areas where they had been seeded. Demonstrators were required to bin detections into six categories, from 1 to 6, with 1 corresponding to most likely UXO and 6 corresponding to most likely clutter. This binning allows a ROC curve to be formed. For the airfield open field area, we have chosen to plot probability of detection on the ordinate and use background alarm rate as the abscissa for two reasons. First, APG is fairly confident that all intact ordnance was cleared from the area, so detections not corresponding to emplaced ordnance are likely clutter. The limited dig at the airfield supports that assumption. Second, this normalizes the detection curves. That is, a demonstrator can achieve a probability of detection of 1.0 simply by having a dense enough set of detection calls. (From a practical point of view, the performance of such a system might be judged much poorer than that of another system with a somewhat smaller probability of detection, but much lower background alarm rate.)

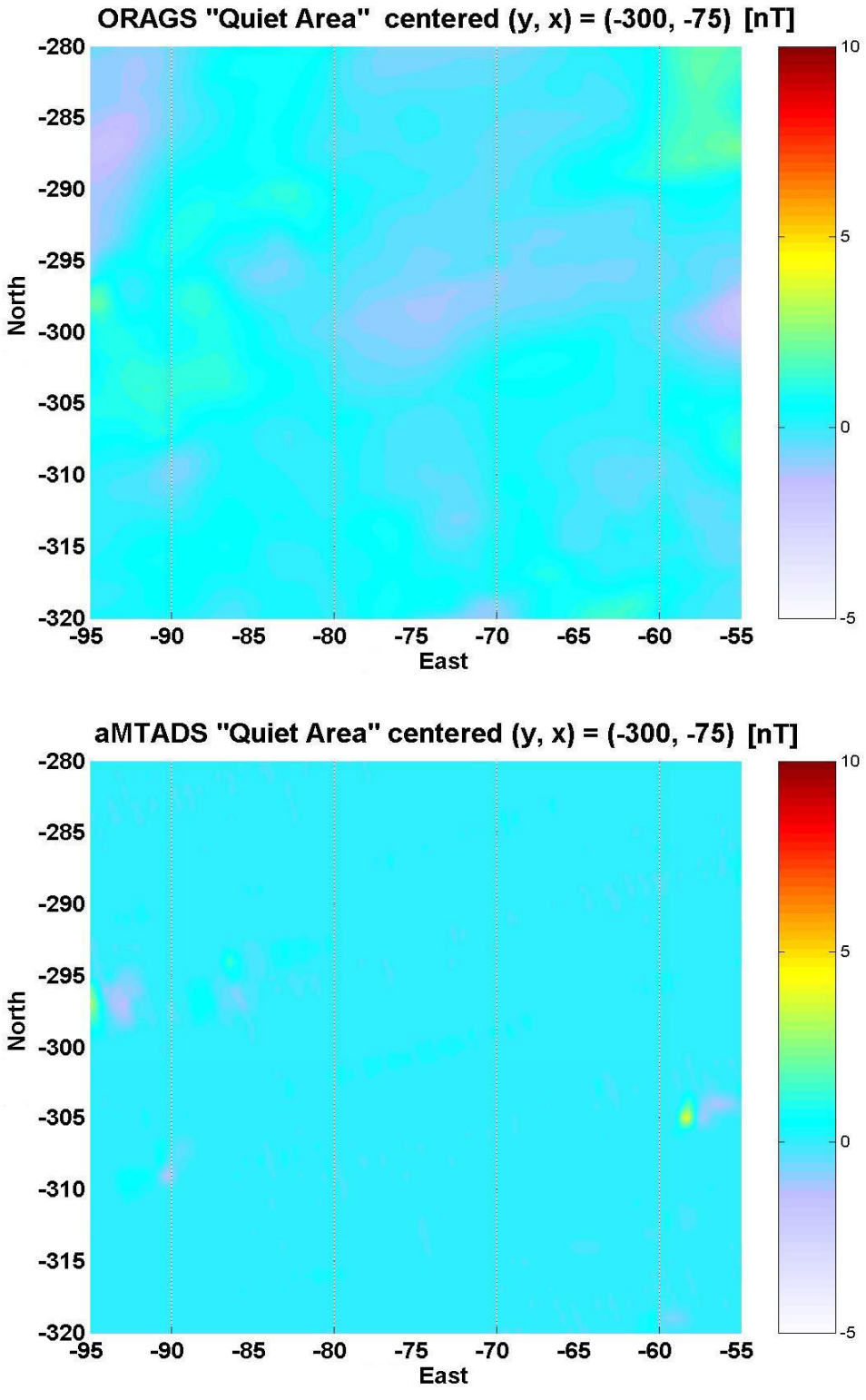

Figure 13. Magnetometer Maps of One Airfield Quiet Area

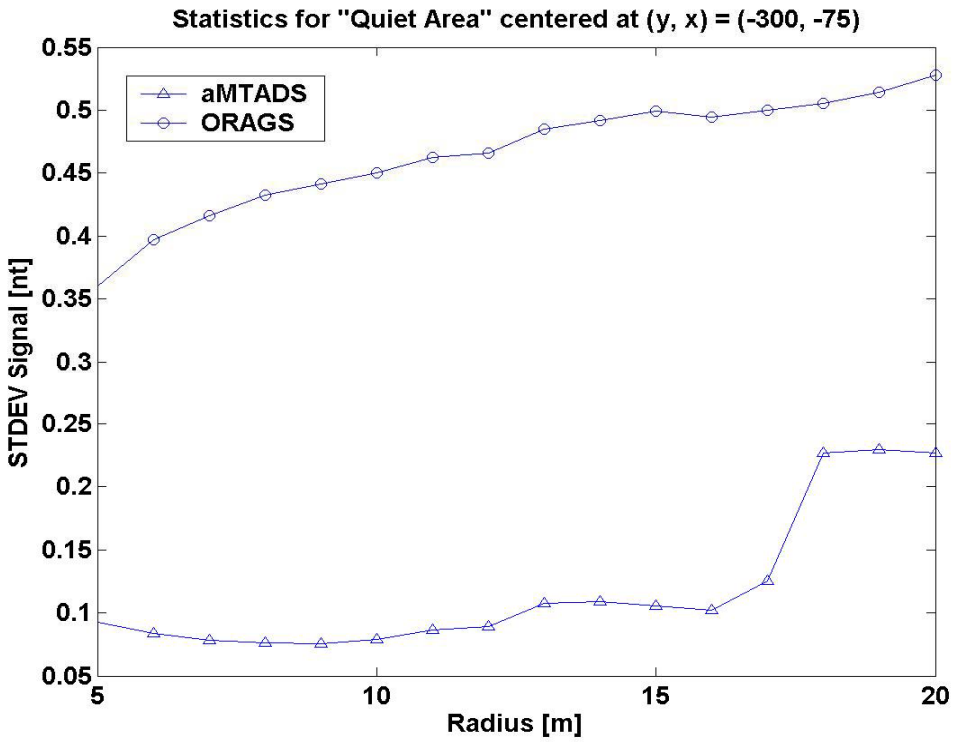

Figure 14. Noise Standard Deviation as a Function of the Radius of the Area Considered for the Quiet Area of Figure 13

Table 7. Peak SNR Values from the Airfield Open Field Area

Target #	Target Type	ORAGS SNR	aMTADS SNR
1	105 mm	89.8	1920.7
2	105 mm	93.3	1368.4
3	105 mm	22.8	355.4
4	81 mm	13.3	269.0
5	81 mm	18.7	275.2
6	81 mm	15.6	63.7

In fact, a demonstrator can achieve a 100% Pd without benefit of a survey. All one has to do is select detection locations such that the halos used for grading detection cover the entire area. For uniform randomly placed detection calls and target locations, we might expect to detect, by chance, a fraction of the targets given by ratio of the area covered by the halos to the surveyed site area. Thus, in general, some portion of the detections credited to a demonstrator will be "true" detections and some will be "chance" [7]. Appendix A provides an analysis that allows us to separate detections into the two categories. After a discussion of the detection performance of both demonstrators, we

apply the true versus chance detection analysis to provide better understanding of the results.

To evaluate detection performance, a circle ("halo") of a chosen radius was created around each of the emplaced ordnance item locations. If a system detection declaration fell on or within the circle, that item was counted as detected. While the term "halo" strictly connotes the circumference of the circle, we instead use the term here to refer to the circle radius, as that is the direct measure of the maximum location error allowed for a detection to be counted. Halos from 0.5 m to 2 m were explored, but based on the target location accuracies of the two systems, most of the results presented are for a 1.5 m halo. Where illustrative, results for 1 m and 2 m halos are also given. Figure 15 provides the ROC curves based on a 1.5 m halo for each system in the airfield open field area. Two curves are provided for the ORAGS system. As noted earlier, ORNL personnel used two different sets of algorithms for detection and discrimination calculations. The curve labeled ORAGS-UV and ORAGS-MV correspond to results from univariate and multivariate detection and classification algorithms, respectively. In this case, the univariate algorithm performed somewhat better than the multivariate. For both algorithms, category 5 and 6 calls included no additional ordnance, and approximately half the detection calls were in those categories. The aMTADS showed substantially better performance in this case than either ORAGS algorithm. However, that performance included 5 of 49 total ordnance detections in category 5 and 1 in category 6.

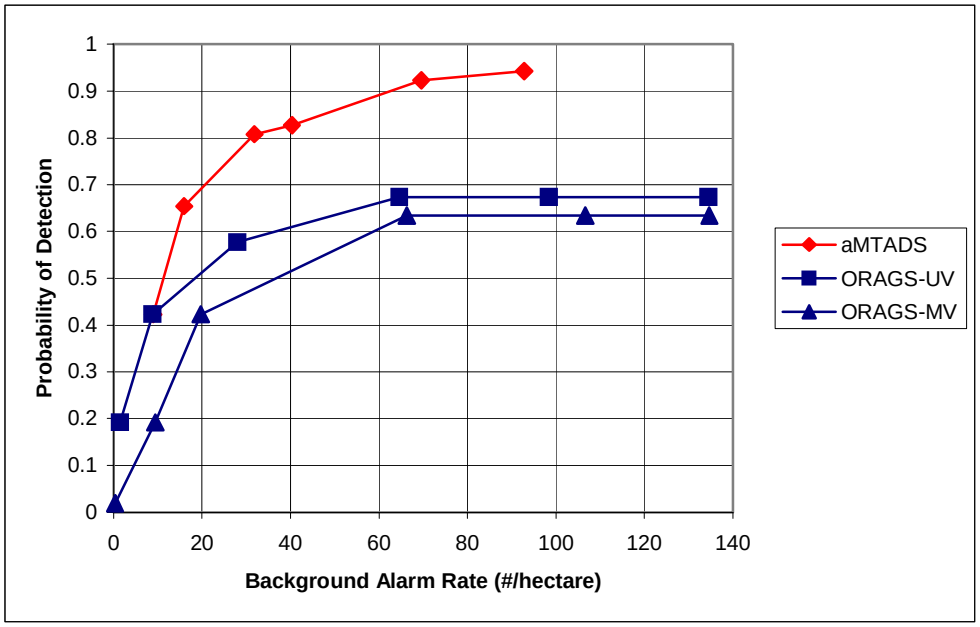

Figure 15. Receiver Operating Characteristics Curves for the Airfield Open Field Area for a 1.5 m Halo

In addition to calculating the ROC curves for the airfield, we analyzed the type of ordnance detected as a function of the halo size for 1 m, 1.5 m, and 2 m halos. Table 8 provides those results. In going from a 1 m to a 2 m halo, only the ORAGS-MV results showed a substantial improvement in detection, rising from 15 percent below the univariate algorithm results to 2 percent above over that range. This is not surprising, due to the east bias of 23.3 cm and a north bias of 39.7 cm in position estimation shown by the multivariate algorithm, compared with 0.7 cm east and 6.4 cm north for the univariate algorithm and –6.1 cm east and 8.4 cm north for aMTADS (see Figure 16). Based on the chance detection analysis for this site, discussed later, the curves in Figure 15 for the 1.5 m halo appear to be representative of relative system performance.

Table 8. Ordnance Detection Results for the Airfield Open Field Area for Three Detection Halos

		ORAGS			aMTADS		
Ordnance	Emplaced	(1 m) UV/MV	(1.5 m) UV/MV	(2 m) UV/MV	(1 m)	(1.5 m)	(2 m)
60 mm	3	2/1	2/2	2/2	3	3	3
81 mm	21	9/7	10/10	12/13	16	18	18
105 mm	28	21/16	23/21	23/23	27	28	28
Total	52	32/24	35/33	37/38	46	49	49

We also created location-error scatter plots for the 1.5 m halo. Figure 16 provides those data for each system. (We don't show the ORAGS-MV algorithm performance, because it was worse than that of the ORAGS-UV algorithm.) The ORAGS-UV detections provided east and north error standard deviations of 42.2 cm and 56.6 cm. For aMTADS, east and north error standard deviations were 27.8 and 36.2 cm.

The radial error is the square root of the sum of the squares of the north and east errors. The airfield data plotted in Figure 16 results in a radial error histogram for each system; these are plotted in Figure 17. If north and east position errors are independent, zero-mean Gaussians with equal variances in the two dimensions, the radial error histogram should show a Rayleigh distribution [8]. That is approximately true of the aMTADS errors in Figure 17. The ORAGS-UV errors, on the other hand, are far from Rayleigh, likely indicating some systematic position errors. The average aMTADS radial error in Figure 17 is 35 cm, while the ORAGS-UV average radial error is 64 cm. The ORAGS-MV data, with its large mean offsets, has an average radial error of 73 cm.

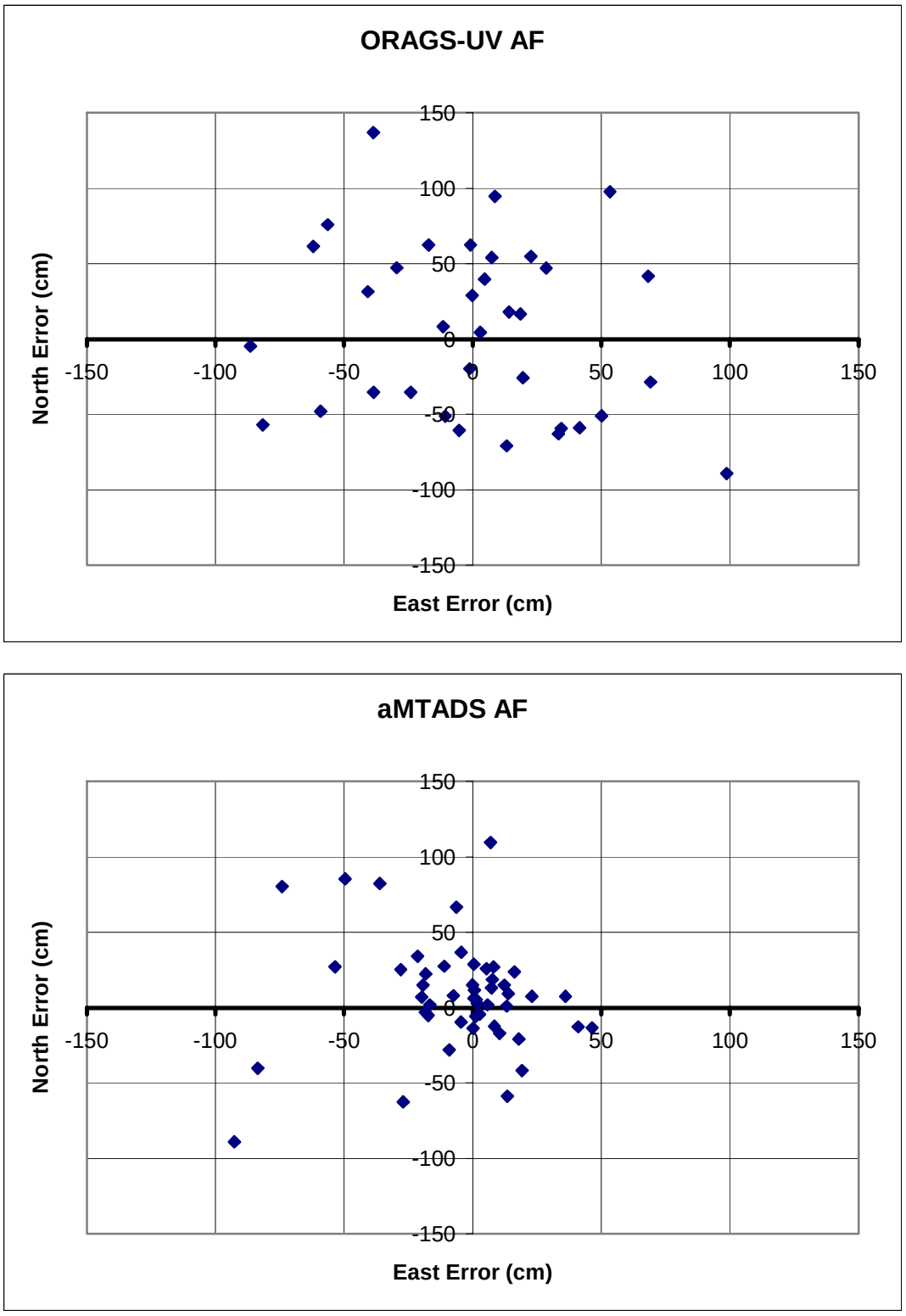

Figure 16. Location Error Scatter Plots for the Airfield Open Field Area

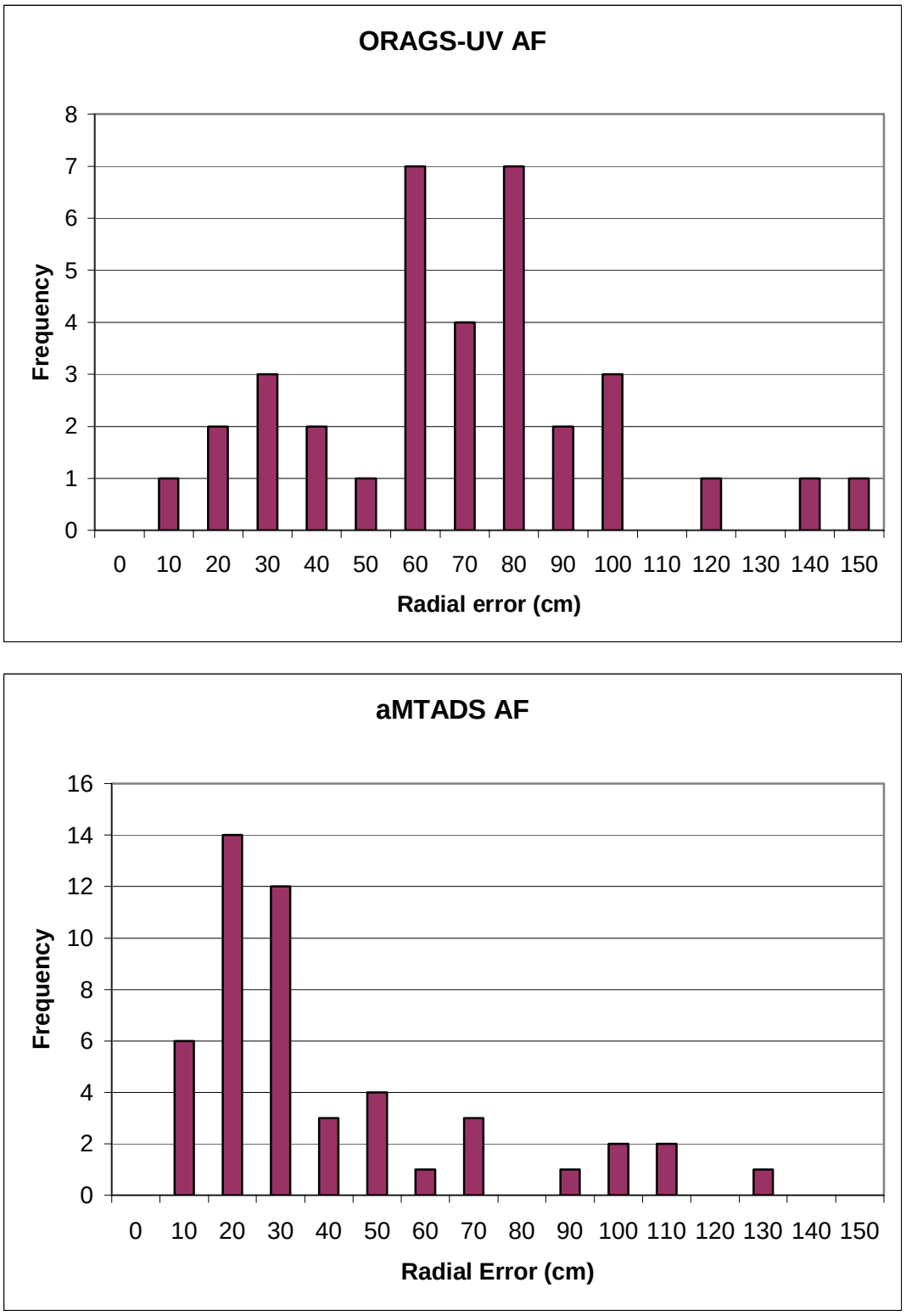

Figure 17. Radial Error Plots for Oak Ridge Airborne Geophysics System-UV and Airborne Multi-Sensor Towed Array Detection System Data from the Airfield Emplaced Ordnance

In the airfield area the total number of declarations by both sets of demonstrators was relatively small (608 for aMTADS and 845 for ORAGS-UV). The site area is 6.02 hectares, which translates to 71 m^2 per pick for ORAGS-UV and 99 m^2 for aMTADS. Figure 18 provides a plot of the detection declarations for both demonstrators, along with the locations of the 52 emplaced UXO items. Because of the scale employed and the symbol size required to be able to see the system declarations and the emplaced items, the plot provides a distorted view of the distance between items. It is not intended to provide a quantitative indication, but instead a qualitative feel for the density of declarations by the two systems and their locations compared with emplaced item locations.

Based on the chance detection model, all 49 of the aMTADS detections would be declared as true detections. For ORAGS, using only the declarations in categories 1–4, (there were no UXO detections in categories 5 and 6), 34 of the 35 univariate and 32 of the 33 multivariate would be declared true detections, with only one UXO detection a chance detection. In the more cluttered areas that was not the case. For the cluttered areas, additional analysis is presented to assess what portion of the total number of detections likely represented chance detections.

Of the three areas where UXO was emplaced, only in the airfield area was the background such that calculation of a detection curve vs. background alarm rate made sense. The dewatering pond geometry made assessment of the area that should be included for background difficult to fairly determine, and, with no subsequent recovery of detected background items, the likely distribution of background alarms between UXO and clutter is unknown. The active field area was highly cluttered, and, based on later recovery data (see Appendix B), many of the background declarations in the active field area would have been ordnance or ordnance-related clutter. For those reasons, only detection of emplaced ordnance was scored in the dewatering pond and active field areas.

In the dewatering ponds area, ordnance emplacement was limited to the large and small ponds interior to the field. Figure 19 [2] is a photograph of the area, and Table 9 provides the number of ordnance emplaced and the number detected by each demonstrator. Figure 20 provides a map of emplaced items and the detection calls by both demonstrators. Only the ORAGS-UV calls are plotted, but the OAGS-MV algorithm produced the same number of detections.

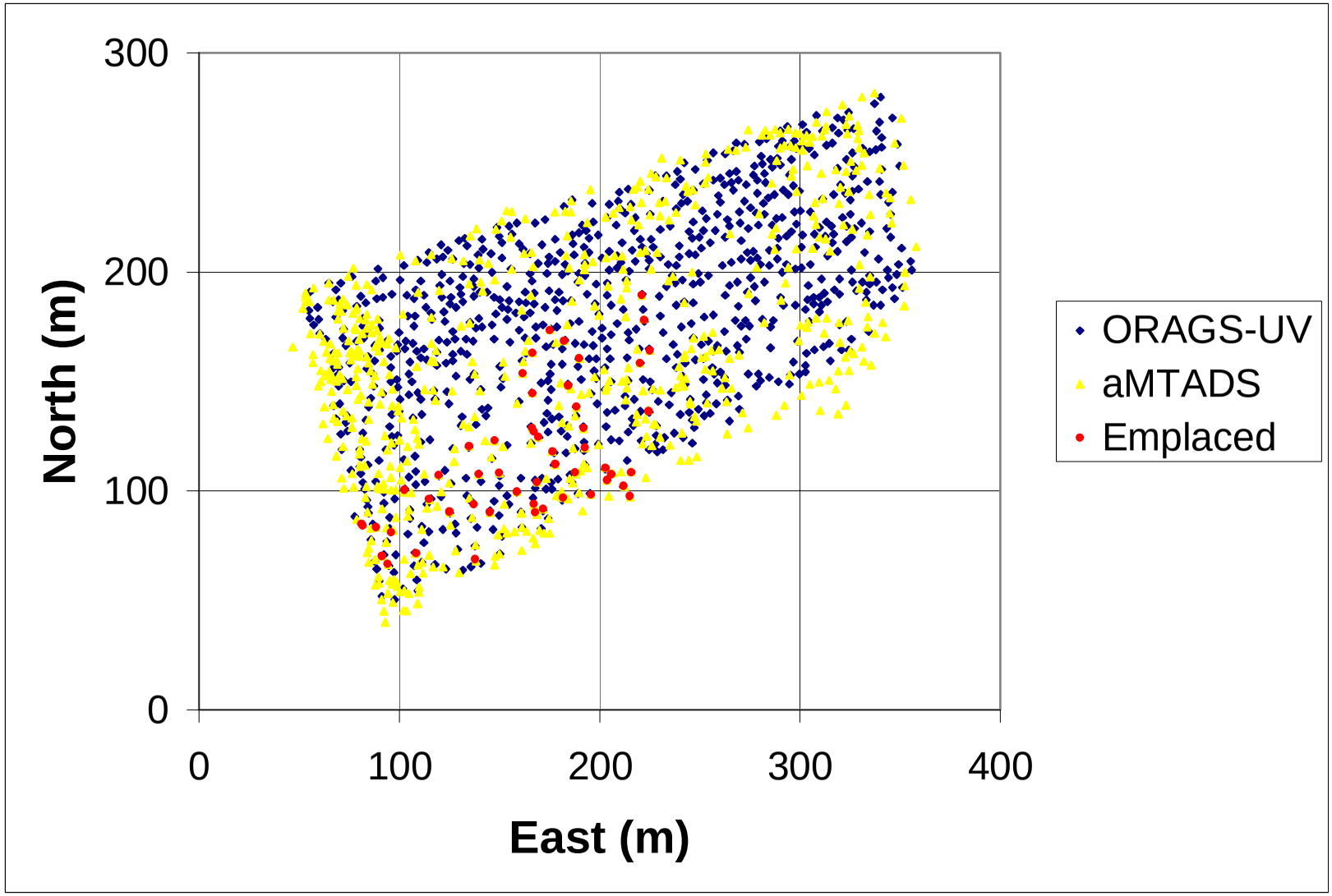

Figure 18. Target Declarations and Emplaced Ordnance Locations for the Airfield Open Field Area

Figure 19. Dewatering Ponds Area [2]

All ordnance items were placed in the ponds, and the aMTADS detections are localized to the ponds and berm areas around the ponds. The ORAGS-UV detections, on the other hand, are spread across the entire area. For that reason, we have chosen not to do a chance detection analysis for this area, as it would be difficult to apply in a manner that could be justified.

The berms around the edges of the ponds restricted the helicopters' abilities to fly close to the pond surface. That, and because the targets were on the pond bottoms and therefore at a greater distance from the sensors than for the airfield case, made detection difficult. The smallest target, the 81 mm, proved particularly difficult, although ORAGS did detect 1 of the 16 emplaced. When normalized for number of ordnance of each type emplaced, the aMTADS results in Table 9 show a detection trend that increases monotonically with ordnance size, as might be expected. ORAGS detected too few ordnance for any trend to be evident.

Table 10 provides the cumulative detection results as a function of UXO likelihood call. The aMTADS results are based on a total of 224 detection calls. Table 10 shows aMTADS making all its detections in the top three UXO likelihood categories and none in categories 4–6. On the surface, that would indicate excellent discrimination capability. In fact, that is not the case, as only 4 of the 224 declarations were in categories 4–6. The ORAGS univariate analysis is based on 2,143 detection calls, and the multivariate analysis is based on 2,140 calls. Note, however, from Figure 20 that most of those declarations were outside the pond areas where UXO were emplaced.

Table 9. Ordnance Detection Results for the Dewatering Ponds for Two Detection Halos

Ordnance	Emplaced	ORAGS		aMTADS	
		(1 m) UV/MV	(1.5 m) UV/MV	(1 m)	(1.5 m)
81 mm	16	1/1	1/1	0	0
105 mm	25	1/1	2/2	10	11
155 mm	6	0/0	0/0	3	4
Total	47	2/2	3/3	13	15

Table 10. Cumulative Detection Probability as Function of Ordnance Likelihood Call for the Dewatering Ponds

UXO Likelihood	ORAGS (UV/MV) % detections		aMTADS % detections	
	1 m halo	1.5 m halo	1 m halo	1.5 m halo
1	0/0	0/0	19.1	19.1
2	0/2.1	0/2.1	25.5	29.8
3	0/2.1	0/2.1	27.7	31.9
4	0/4.3	2.1/4.3	27.7	31.9
5	2.1/4.3	4.3/6.4	27.7	31.9
6	4.3/4.3	6.4/6.4	27.7	31.9

The final area with emplaced ordnance was the active recovery field (see Figure 21 [2]). There, ordnance was emplaced in an open field, among the phragmites, and in the littoral area. Note the heavy concentrations of scrap piles. As an active recovery field for indirect weapons fire, this area is very heavily cluttered with ordnance and ordnance fragments. Figure 22 provides a plot of ORAGS-UV and aMTADS anomaly selections, along with the locations of emplaced items

Only 81 mm and 105 mm shells were used as emplaced ordnance. Tables 11 and 12 provide target detection results by ordnance type and as a function of UXO likelihood call. Because of high residual clutter, neither system performed particularly well at Active Recovery Field, but ORAGS detected twice as many total targets as aMTADS.

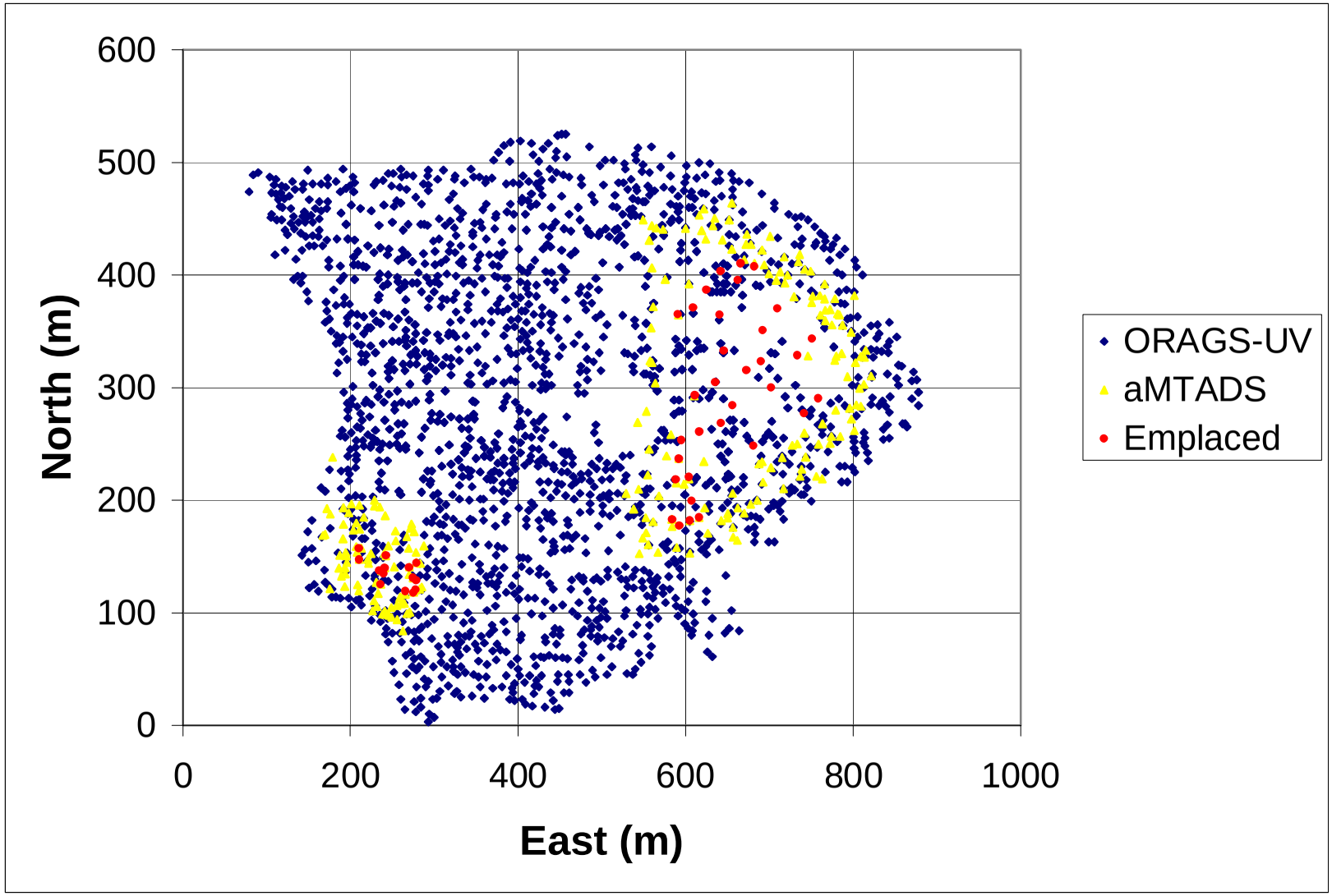

Figure 20. Target Declarations and Emplaced Ordnance Locations for the Dewatering Ponds

Figure 21. Active Recovery Field Area [2]

Table 11. Ordnance Detection Results for Active Recovery Field for Two Detection Halos

Ordnance	Emplaced	ORAGS		aMTADS	
		(1 m) UV/MV	(1.5 m) UV/MV	(1 m)	(1.5 m)
81 mm	32	2/2	4/4	0	1
105 mm	32	6/6	6/6	4	4
Total	64	8/8	10/10	4	5

Table 12. Cumulative Detection Probability as Function of Ordnance Likelihood Call for Active Recovery Field

UXO Likelihood	ORAGS (UV/MV) % detections		aMTADS % detections	
	1 m halo	1.5 m halo	1 m halo	1.5 m halo
1	0/0	0/0	3.1	4.7
2	3.1/0	3.1/0	4.7	6.3
3	9.4/0	9.4/0	4.7	6.3
4	9.4/1.6	9.4/1.6	6.3	7.8
5	10.9/9.4	12.5/9.4	6.3	7.8
6	12.5/12.5	15.6/15.6	6.3	7.8

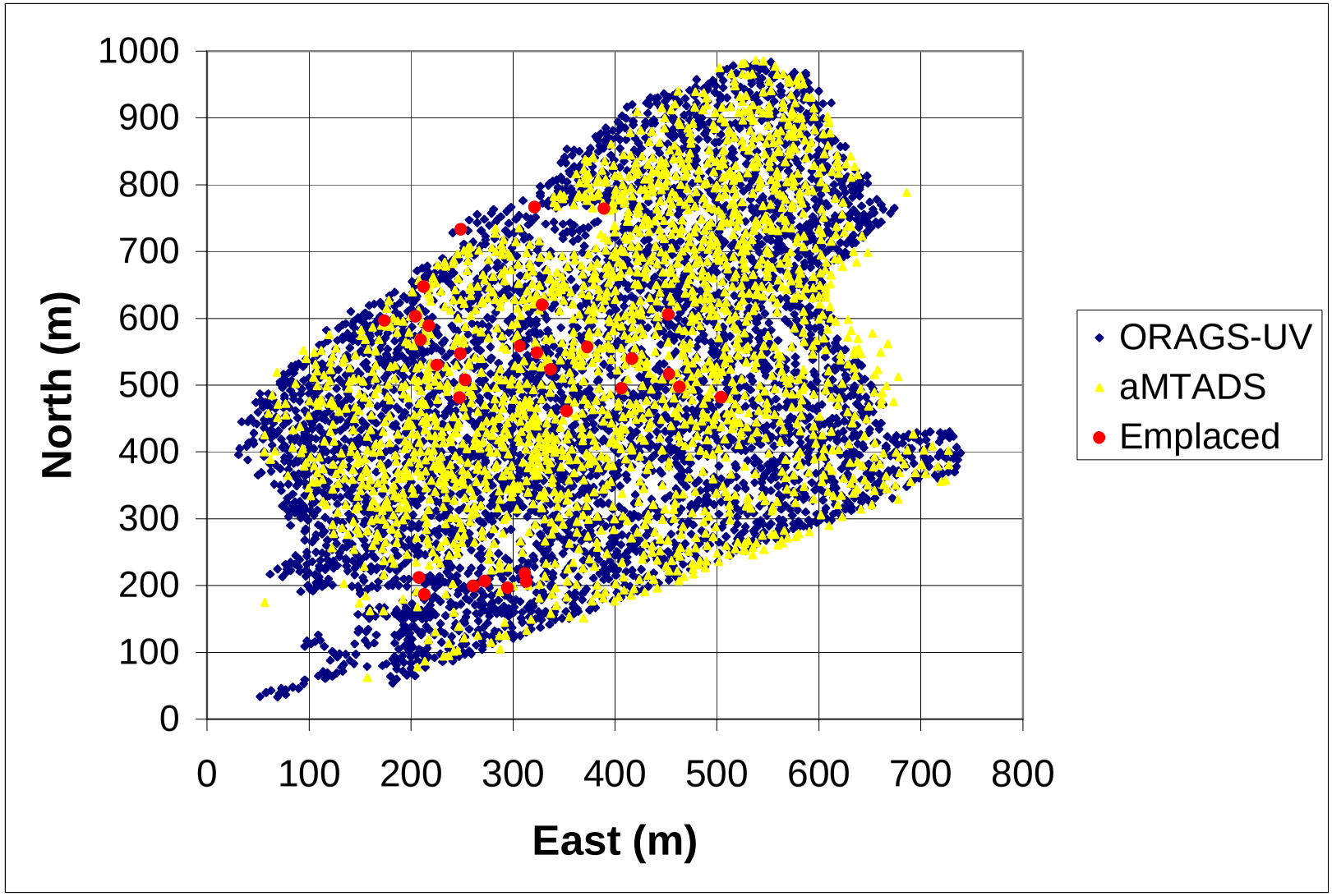

Figure 22. Target Declarations and Emplaced Ordnance Locations for the Active Recovery Field Area

The formula for true matches was applied to the results from the active recovery Field site graded for the 1.5 m halo case. The univariate results were used for ORAGS because that algorithm never fared worse than the multivariate algorithm and provided better location accuracy. Table 13 provides the results of the analysis. The solution to the equation is rounded to the nearest integer. A calculation is done for each of the six ordnance likelihood categories.

Table 13. Assessment of True Detection Statistics for the Active Recovery Field Site

UXO likelihood	Cumulative Number of Declarations (ORAGS/aMTADS	ORAGS-UV		aMTADS	
		Detections	True detections	Detections	True detections
1	117/759	0	0	3	2
2	804/1628	2	1	4	2
3	2257/1914	6	2	4	2
4	3877/1970	6	2	5	3
5	4676/1996	8	3	5	3
6	4879/1996	10	5	5	3

For the highly cluttered active recovery field, both systems detected a large number of anomalies: ORAGS-UV declared 4,879 total detections, and aMTADS declared 2,968. Because about a thousand of the aMTADS declarations were in the littoral region where ORAGS did not fly, only the 1,996 declarations shown on Figure 22 were used in the chance detection analysis. Although the active recovery field is a 42.1 hectare site, the large number of declared detections resulted in ORAGS calls covering 8.2% of the total area for a 1.5 m halo and aMTADS calls covering 3.4%. Because of the small percentages of ordnance detected—especially given the percentage of site coverage—it is not surprising that 50% of the ORAGS and 40% of the aMTADS detections were likely by chance.

In addition to emplaced UXO at the active recovery field site, a selected number of items detected by both demonstrators were recovered and classified. IDA created an ordered dig list comprising targets in the higher UXO likelihood categories (1-3) for each demonstrator that matched a target location on the other demonstrator's list. Targets were only included if the locations on the two lists were within 0.5 m of each other. Preference was given to targets with a high UXO likelihood category on both lists, but a significant number of choices differed significantly in UXO likelihood between the two lists. To reduce ambiguity, we attempted to provide matched pairs that were well separated from

other detections. The average distance to the next nearest detection was 6 m, but a few items had nearest neighbors less than 0.5 m away. (Some additional off-shore targets were also dug, but we have not included them in this analysis.) In assessing the detection response for the dug items, a 1.5 m halo has been used relative to the actual dug location of the excavated items, not the originally provided coordinates. In scoring discrimination, the recovered items have been classified as intact ordnance (O), ordnance-related (OR), or clutter (C). Some items were listed as having unreliable recovery data or had no description. Those were also not included in the analysis. Figure 23 shows the dug item locations, and Appendix B provides a list of the items, with locations relative to the coordinates of Figure 23. Note the heavy preponderance of ordnance and ordnance-related items in the list, where we have classified 46 items as ordnance, 56 as ordnance-related, and only 16 as clutter.

Because all the dug items were chosen from items that appeared on both detection lists, we would expect the probability of detection to be near unity, and that is the case. Both systems had a detection within a 1.5 m halo for 115 of the 118 items. The two systems missed the same 3 items (2 ordnance and 1 clutter), in every case because the actual coordinates of the dug item were more than 1.5 m from the dig list coordinates provided and were not within 1.5 m of a declaration on either list.

Figures 24 and 25 provide ROC curves, based solely on the items of Appendix B. Two cases have been calculated: (1) only intact ordnance counted as UXO and (2) intact ordnance and ordnance-related items counted as UXO. Figure 24 shows ROC cures for the first case. Here, ordnance-related clutter and clutter are included in the false-alarm category. Figure 25 provides ROC curves for the second case. Here, false alarms are the non-ordnance-related clutter. For both cases, all the items matched in the Appendix B list were matched by aMTADS category 1-3 detections, and ORAGS-UV had detections in all six categories. aMTADS performs somewhat better than ORAGS-UV in the first case, but it is worse for the second case. In neither case does the performance ever rise substantially above the chance diagonal. The data likely only illustrate the difficulty of classification for an airborne magnetometer, with its wide single-sensor footprint, in a highly cluttered area like the active recovery field.

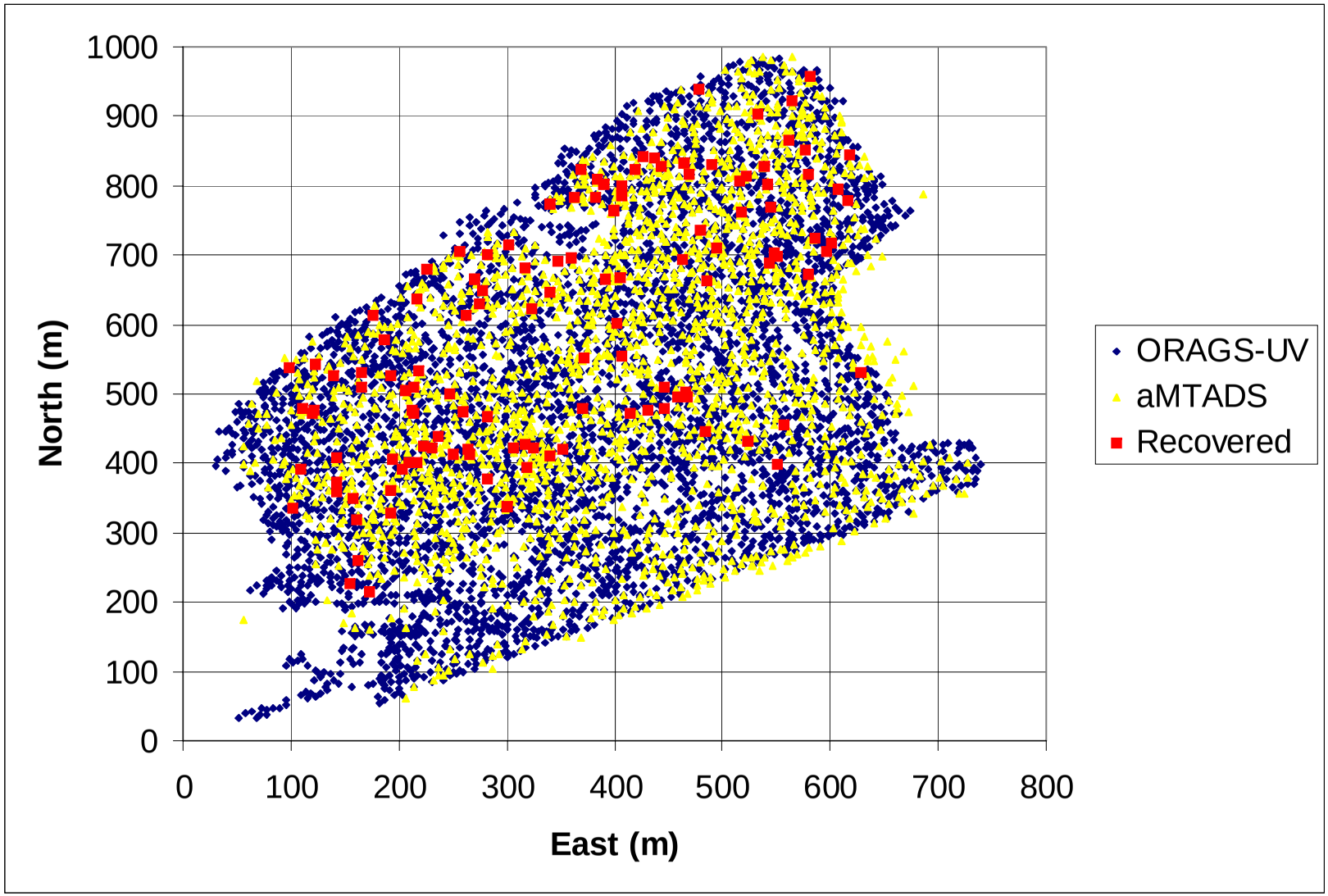

Figure 23. Target Declarations and Recovered Target Locations for the Active Recovery Field Area

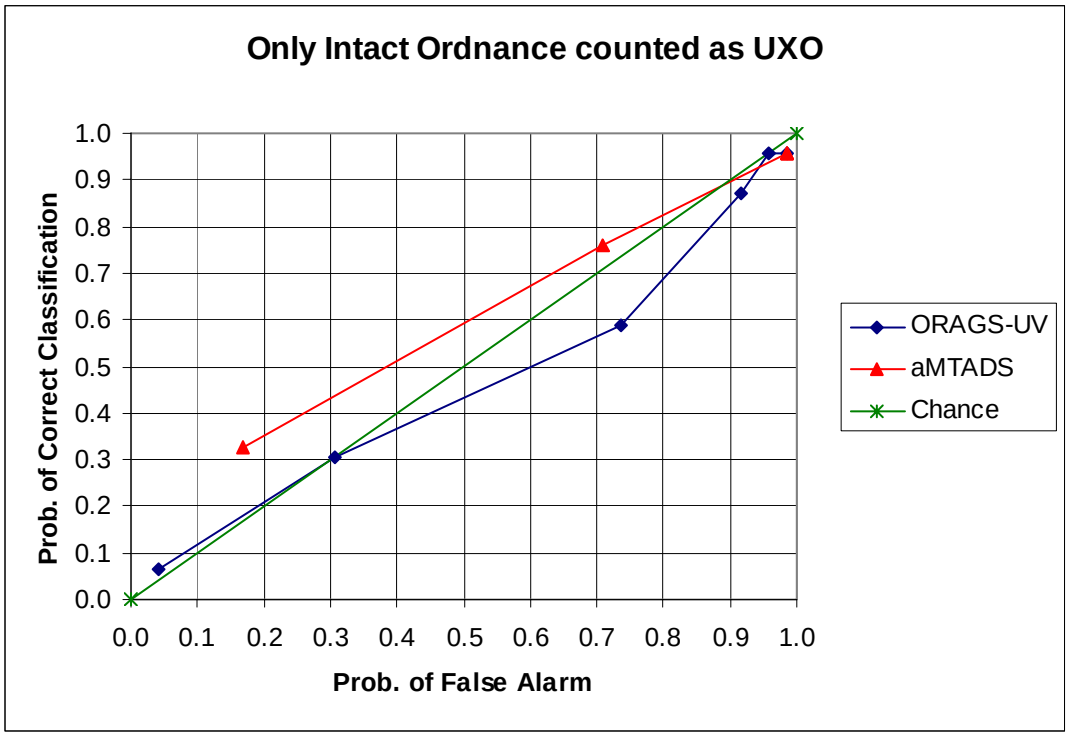

Figure 24. Receiver Operating Characteristic Curves for the Active Recovery Field Dug Items Where Only Intact Ordnance is Counted Toward Probability of Correct Classification

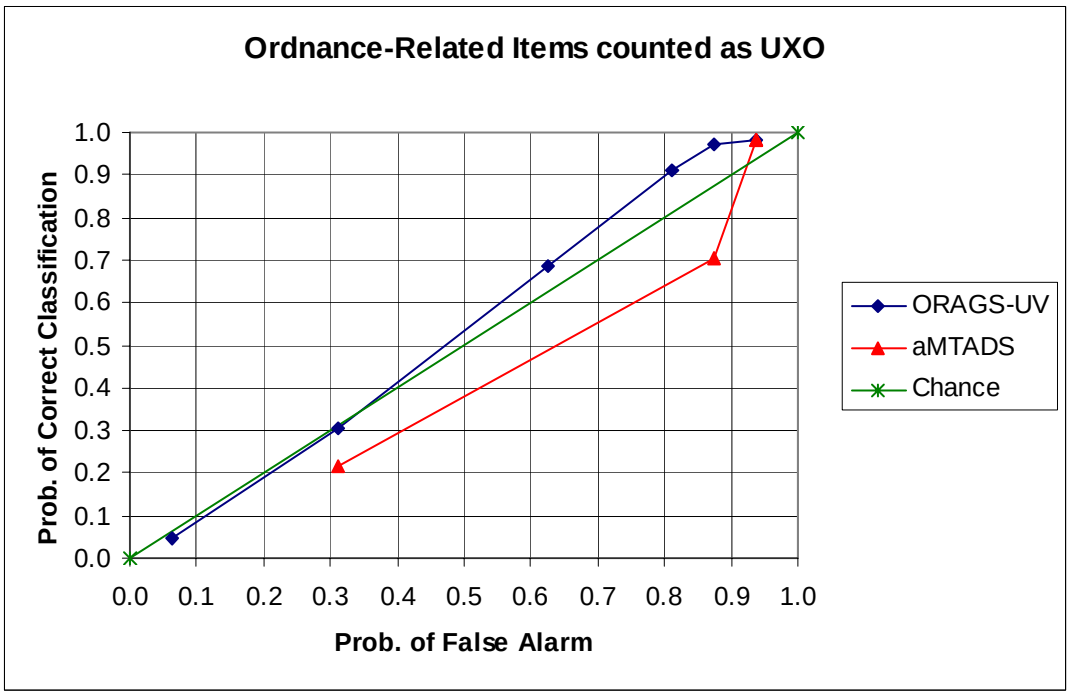

Figure 25. Receiver Operating Characteristic Curves for the Active Recovery Field Dug Items Where Intact Ordnance and Ordnance-Related Clutter are Counted Toward Probability of Correct Classification

III. FINDINGS AND CONCLUSIONS

A. FINDINGS

The demonstrations analyzed in this report were designed to test the detection and classification capabilities of airborne magnetometer systems over a wide range of terrain types and levels of background clutter. UXO was emplaced in selected areas to provide known items against which system performance could be judged. This report focuses on overall performance, which is a function of a number of factors. These include, as a minimum, inherent sensor sensitivity, sensor footprint, proximity to the target, spatial sampling densities in down- and cross-track, target location accuracy, and signal processing. Signal processing comprises prefiltering for background variation removal, interference reduction and sensor output leveling, target location (whether manual or automatic), and classification processing.

These two systems employ the same model cesium vapor magnetometers carried on identical helicopters. Although the details of the electronics differ between the systems, we would expect their inherent signal sensitivities to be similar, and that was the case for the calibration targets and airfield targets analyzed in this report. While the aMTADS typically produced a signal level two to five times that of ORAGS, this can be explained by the difference in helicopter altitudes flown during the survey.

The inherent noise floors for the two systems, inferred from the high-altitude data, also appear to be very similar, but current ORAGS processing provides four or five times more background variation over quiet areas in low-altitude flight than does aMTADS. The combination of the lower flight altitudes and better noise suppression gave aMTADS an average SNR advantage against comparable targets of a factor of 10 in the calibration area and 17 in the open field area of the airfield.

The other two scored areas presented much more difficult problems for both systems than did the flat, relatively uncluttered airfield area. The dewatering ponds would have been challenging under the best of circumstances because of the separation between the sensors and the targets. Only 10 of the 48 emplaced ordnance items were a foot or less below the water surface, with 31 of the items 3 feet deep or more, and 18 of the items 6 or more feet deep. In addition, berms around the ponds made it difficult for the pilots to fly close to the surface, particularly near the edges of the ponds. Qualitative reports from

the demonstrators indicate that aMTADS was able to fly lower over the ponds than ORAGS—this shows in the detection results, where ORAGS detected only 3 emplaced items but aMTADS detected 15. However, 10 of the 15 aMTADS detections were 2 feet deep or less and the 1 very deep item (a 155 mm shell, 5.5 feet deep) and 1 item 3 feet deep were likely chance matches, as the aMTADS location errors were more than 1 m. In normal land-clearance operations, deep UXO items are also typically massive, so that signature somewhat offsets the distance falloff. In the water, that is not the case, and airborne or surface magnetometer systems are likely to be effective only for very shallow bodies of water or where only very large targets are of interest.

The active recovery field is a very cluttered site, and the results there confirm the generally acknowledged feeling that effective clearance of buried items in such situations requires clearance of surface clutter beforehand. Neither system did well in detecting emplaced items, and around half the items detected by both systems were likely detected by chance.

B. CONCLUSIONS

Several conclusions can be drawn from the results of these demonstrations:

- If maximum sensitivity is desired, it is important that the system design allow very low-level flight in areas where that is possible. Careful attention to reducing apparent spatial background variations caused by platform dynamics effects is also crucial in obtaining maximum detection sensitivity. In the very benign airfield terrain and background, aMTADS detected 49 of 52 emplaced items, including all three 60 mm mortars and eighteen of twenty-one 81 mm mortars, but ORAGS, flying about a meter higher and 3 times as fast, and with 4 times the background standard deviation, detected 14 fewer emplaced items, missing one of the 60 mm, 11 of the 81 mm, and 5 of the 105 mm.
- Successful detection of UXO targets in bodies of water will require knowledge of the burial depth and types of ordnance expected. Helicopter systems such as these already have the disadvantage of a sensor that is a meter or two above the surface. Because of the $1/(\text{distance})^3$ signal falloff, even moderate target depths make the detection of all but large targets marginal.
- Neither system shows significant individual target-detection capability in highly cluttered areas.
- Target location accuracy is important for unambiguous target recovery. aMTADS demonstrates that average radial position errors of less than 40 cm are possible from an airborne system using real-time, differential GPS.

However, obtaining that degree of accuracy requires reliable sensing and precise accounting for helicopter dynamic effects on sensor position.

- Accurate automatic detection and classification algorithms would be of significant benefit for systems, such as the ones demonstrated here, that are capable of surveying hundreds of acres per day. Current automatic algorithms, however, do not perform as reliably as human analysts. Particularly in the detection phase, they result in many more anomalies that would have to be dug, without adequate discrimination capability to make up for the additional detections.
- Current-generation helicopter-borne magnetometer systems are capable of reliably detecting areas of high ferrous clutter/UXO density. It appears they are not suitable for general survey use to detect individual ordnance items, except in special conditions that provide a combination of benign terrain, low background clutter, and appropriate UXO sizes (>60 mm). Even then, lower and slower flight than indicated in system specifications will likely be required to achieve adequate detection performance.

ACRONYMS

aMTADS	Airborne Multi-Sensor Towed Array Detection System
APG	Aberdeen Proving Ground
ESTCP	Environmental Security Technology Certification Program
FFT	fast Fourier transform
GPS	Global Positioning System
HAE	height above ellipsoid
IDA	Institute for Defense Analyses
MTADS	Multi-Sensor Towed Array Detection System
NRL	Naval Research Laboratory
ORAGS	Oak Ridge Airborne Geophysics System
ORNL	Oak Ridge National Laboratory
Pd	probability of detection
ROC	receiver operating characteristic
SERDP	Strategic Environmental Research and Development Program
SNR	signal-to-noise ratio
STDEV	Standard deviation
UTM	Universal Transverse Mercator
UXO	unexploded ordnance

REFERENCES

[1] *2002 Airborne Geophysical Survey at Aberdeen Proving Ground, Maryland,* prepared by the Environmental Sciences Division, Oak Ridge National Laboratory, Final Report Revision 0 on ESTCP Project 200037 and 37, August 2004.

[2] McDonald, J.R., et al., *Airborne MTADS Demonstration at the Aberdeen Proving Ground, July 2002*, NRL draft Demonstration Report on ESTCP Project 200031, 25 May 2003.

[3] Rowe, Gary, *Wide-Area UXO Technology Demonstration and Survey*, U.S. Army Aberdeen Test Center Report ATC-8716, dated November 2003.

[4] *Wide Area UXO Aerial Demonstration and Survey*, Powerpoint presentation prepared by the U.S. Army Environmental Center, undated.

[5] *Demonstration and Comprehensive Mission Plan, Airborne Magnetic Surveys at the Aberdeen Proving Ground*, prepared by the Environmental Sciences Division, Oak Ridge National Laboratory, Revision 1, 24 June 2002.

[6] *Technology Demonstration Plan, Airborne MTADS Demonstration Over Selected Test Sites at the Aberdeen Proving Ground*, draft prepared by the Naval Research Laboratory, 24 June 2002.

[7] Altshuler, T., et al., *Demonstrator Performance at the Unexploded Ordnance Advanced Technology Demonstration at Jefferson Proving Ground (Phase I) and Implications for UXO Clearance*, IDA paper P-3114, October 1995.

[8] Papoulis, A., *Probability, Random Variables and Stochastic Processes,* McGraw-Hill, 1965, p. 195.

APPENDIX A
CHANCE DETECTION ANALYSIS

In analyzing detection performance, evaluators long ago realized that some number of detections were likely to be due to chance. That is, a certain number of detections that are graded as true detections are not actually associated with the item assumed to be detected. To illustrate the point, if N detection calls were randomly distributed over a test plot with area A, a demonstrator might expect, just based on chance, to achieve an apparent probability of detection approximately equal to $N\pi R_h^2/A$, where R_h is the radius of the halo used. A more sophisticated analysis is developed in Reference 7 to assess the number of these "chance" detections. The assumption made is that the survey instrument has inherent random errors in locating targets that can be described by zero-mean and equal variance Gaussian distributions in two orthogonal dimensions. For that assumption, we would expect the probability density function for the radial error to be Rayleigh and the probability of detecting an object within a radius R_h of the declared location would be given by [8]:

$$P(z \le R_h) = \int_0^{R_h} \frac{z}{\sigma^2} e^{-z^2/2\sigma^2} = 1 - e^{\frac{-1}{\sqrt{2}}\left(\frac{R_h}{\sigma}\right)^2},$$

where σ is the location error standard deviation in the east and north directions. If the halo is substantially larger than the error standard deviation, then the probability that a detected target lies inside the halo is essentially unity. For example, for an $R_h/\sigma = 2$, the probability is 94%, and for $R_h/\sigma = 2.5$, it is 99%. From the airfield emplaced object detections, the worst dimension location error standard deviations were 57 cm for ORAGS-UV and 37 cm for aMTADS. The 1.5 m standard halo used in the APG analysis is more than 2.5 times the ORAGS standard deviation, and so approximating the probability as unity is reasonable. Applying that approximation to the analysis gives the number of "true" detections as

$$T = M - U \cdot F \cdot \alpha$$

where

T = number of true matches

U = true number of missed detections = $B - T$

B = number of items buried

F = true number of false detections = $D - T$

D = number of target declarations

α = (area of halo)/(area of site)

M = Sum of true + lucky matches

This results in a quadratic in T whose solution is

$$T = \frac{-\left(\frac{1}{\alpha} - B - D)\right) + \sqrt{\left(\frac{1}{\alpha} - B - D\right)^2 - 4\left(BD - \frac{1}{\alpha}M\right)}}{2}$$

Curves of true detections as a function of halo should increase as halo size increases and reach an asymptotic value that is indicative of sensor detection performance. For a sensor that produces small position estimation errors, the curve rises rapidly to its final value, but for a sensor with less accurate positioning, the curve reaches asymptote more slowly. When actual data are plotted, however, curves of true detections reach a peak value and eventually start to decrease with increasing halo. The apparent decrease is due to a violation of the assumptions under which the above equations were derived. The analysis assumes that declarations are widely enough separated so that halos never overlap and portions of halos never lie outside the analysis area. At some point, those assumptions break down and the number of chance detections does not continue to rise proportionally to the halo area, so more chance detections are calculated than actually occur. However, until the assumptions are violated, the above development gives a good estimate of true versus chance detections.

APPENDIX B
TABLE OF ACTIVE RECOVERY FIELD DUG ITEMS

East	North	Description	Class.*
223.41	424.19	8-inch projectile, unfired (salute rd)	O
319.11	393.71	2.75 in rocket warhead fired, unfuzed	O
306.03	422.30	155-mm projectile fired, fuzed 3 fragments	O
208.98	401.04	1/2 of 105-mm casing	O
556.49	455.45	155-mm projectile, fuzed, fired	O
275.28	628.87	90-mm projectlie, fuzed, fired	O
109.63	390.62	1/2 of 90-mm casing	O
479.18	736.80	Projectile frag (90-mm) /w fuze	O
262.99	612.22	120-mm projectile fuzed, fired	O
110.96	479.15	5-inch projectile fired, unfuzed	O
121.42	477.00	155-mm projectile fuzed, fired	O
193.45	328.07	90-mm projectile	O
120.64	472.48	105mm projectile, fired, fuzed	O
369.27	822.32	155-mm projectile, fuzed, fired	O
247.81	500.27	155-mm projectile fuzed, fired	O
484.97	446.24	6-inch projectile, fuzed, fired	O
617.72	843.72	90-mm projectile casing, unfuzed	O
543.62	687.75	Low-order 90 or 105 mm projectile	O
266.17	412.38	5-inch projectile, unfuzed, fired	O
606.78	795.06	175-mm projectile, fuzed, fired	O
226.16	679.12	90-mm projectile, fuzed, fired	O
256.49	705.08	155-projectile	O
123.01	541.92	Fuzed 155-mm projectile	O
522.12	813.25	75-mm projectile, fuzed, fired	O
161.44	317.91	155-mm projectile, fuzed, fired	O
186.54	577.60	155-mm projectile unfuzed fired	O
551.30	697.65	75-mm projectile, fuzed, fired	O
372.19	552.56	120-mm projectile fuzed, fired	O
579.39	816.16	75-mm projectile, fuzed, fired	O
348.12	692.21	14-in fuzed projectile	O
140.14	525.22	120-mm projectile fuzed, fired	O
478.76	938.70	155-mm projectile, fuzed, fired	O
218.83	532.54	155-mm projectile unfuzed fired	O
339.30	646.63	155-mm projectile, fuzed, fired	O
259.46	473.42	90-mm AP round fired large piece of scrap metal	O
581.53	958.10	155-mm fired fuzed	O
277.83	647.49	90-mm projectile, unfuzed fired large fragment	O
302.18	714.75	90-mm projectile, fuzed	O
406.45	555.34	120-mm projectile fuzed, fired	O
251.01	411.91	106-mm RAP round	O
98.04	538.35	90-mm projectile, fuzed fired	O
142.98	373.49	240-mm projectile, fuzed, fired	O
597.03	705.65	8-in projectile, fuzed, fired	O
437.16	840.02	155-mm projectile, fuzed, fired	O
404.67	667.36	155-mm projectile, fuzed, fired	O
446.50	479.29	8-inch projectile	O

East	North	Description	Class.*
281.98	466.83	Fragment	OR
431.47	477.14	Fragment	OR
418.39	823.22	Fragment	OR
193.12	526.42	Fragment	OR
494.58	709.45	Fragment	OR
458.00	495.14	Fragment	OR
164.95	509.67	Fragments	OR
426.15	841.09	Large piece of fragment	OR
165.95	529.83	Fragment	OR
545.40	769.32	Projectile fragments	OR
383.05	782.73	Bomb plug	OR
212.03	477.58	Fragment	OR
542.59	802.26	Fragment	OR
615.89	778.97	Fragments from 90-mm projectile	OR
391.97	665.92	Large, thin-wall (bomb?) fragment; unable to recover	OR
192.80	362.00	Fragment	OR
316.63	425.90	105-mm fragment	OR
577.30	851.89	Fragment	OR
561.10	866.51	Fragment	OR
263.50	419.50	Fragment	OR
216.37	401.33	Fragment	OR
370.46	478.64	Fragment	OR
532.23	902.46	Fragments	OR
142.81	408.81	Rod Fragments	OR
538.23	827.30	155-mm fragment	OR
194.12	405.00	Fragment	OR
390.34	802.84	Fragments	OR
407.31	800.08	Fragments	OR
443.29	828.84	Steel fragment	OR
203.26	391.47	Fragments	OR
363.07	782.14	Fragment	OR
352.79	419.07	Fragment	OR
206.64	504.73	Fragments WP projectile	OR
142.86	358.70	Fragments (low order det.)	OR
383.51	810.01	Fragment	OR
214.29	471.37	Fragment	OR
236.34	437.58	Fragment	OR
299.94	338.36	Fragments	OR
316.67	681.99	Suspect ammo burial pit - pipe and fragments	OR
523.79	430.45	Fragments and rebar	OR
176.14	613.47	Fragments	OR
515.70	805.46	Fragment	OR
158.23	349.03	155-mm projectile frag	OR
469.78	817.00	Fragment	OR
485.03	662.36	Fragment	OR
548.66	702.03	Bomb fragment	OR
339.31	411.05	Fragments	OR
213.59	509.98	Fragments (3) possible WP	OR
230.32	422.72	Frag, base of 155	OR
629.01	531.30	Fragments	OR
325.27	422.06	Fragment	OR
550.58	398.03	Small fragments	OR
402.80	601.80	Fragments	OR
564.24	922.80	Fragments	OR
467.91	494.34	Fragment	OR
173.05	214.61	Fragment	OR

East	North	Description	Class.*
462.93	693.36	Cylinder	C
360.27	695.46	Steel plate	C
323.88	623.51	Large piece of angle iron	C
601.84	717.23	Railroad spike	C
465.53	503.12	Railroad rail on end	C
217.09	637.17	steel core ground rod, approx 0.6 meters bent to ground surface ~1.2 m in ground	C
465.27	831.50	Steel plate ring	C
282.40	377.21	Steel plate	C
445.86	509.04	Rebar in concrete	C
414.85	472.83	Pipe and ring	C
154.26	227.10	Household waste pile, metal pitcher, cups, wash buckets, misc. scrap metal	C
580.51	672.81	Large piece of 4" (102-mm) angle iron	C
517.61	761.81	Two metal rods	C
490.34	831.32	Scrap metal	C
101.77	334.25	Scrap metal	C
162.63	260.44	Steel plate	C

* O = Ordnance
OR = Ordnance Related
C = Clutter

REPORT DOCUMENTATION PAGE

Form Approved
OMB No. 0704-0188

1. REPORT DATE	2. REPORT TYPE	3. DATES COVERED *(From–To)*
July 2004	Final	October 2003–July 2004

4. TITLE AND SUBTITLE

Analysis of Airborne Magnetometer Data from Tests at Aberdeen Proving Ground, Maryland, July 2002

5a. CONTRACT NUMBER
DASW01 04 C 0003

5b. GRANT NUMBER

5c. PROGRAM ELEMENT NUMBER

6. AUTHOR(S)

Michael Tuley, Elvis Dieguez, John Biddle

5d. PROJECT NUMBER

5e. TASK NUMBER
AM-2-1528

5f. WORK UNIT NUMBER

7. PERFORMING ORGANIZATION NAME(S) AND ADDRESS(ES)

Institute for Defense Analyses
4850 Mark Center Drive
Alexandria, VA 22311-1882

8. PERFORMING ORGANIZATION REPORT NUMBER

IDA Document D-3015

9. SPONSORING / MONITORING AGENCY NAME(S) AND ADDRESS(ES)

DUSD(SERDP/ESTCP)
901 N. Stuart Street
Suite 303
Arlington, VA 22203

10. SPONSOR/MONITOR'S ACRONYM(S)

11. SPONSOR/MONITOR'S REPORT NUMBER(S)

12. DISTRIBUTION / AVAILABILITY STATEMENT

Approved for public release; distribution unlimited. (23 November 2004)

13. SUPPLEMENTARY NOTES

14. ABSTRACT

The purpose of this technical document is to provide results of IDA's evaluation of data collected by the Naval Research Laboratory (NRL) and the Oak Ridge National Laboratory (ORNL) airborne magnetometer systems in testing conducted at Aberdeen Proving Ground (APG), Maryland, during July 2002. We first give a brief description of the test areas and the data collected. We then summarize the detailed analysis to allow the reader to understand the basis upon which conclusions are drawn.

15. SUBJECT TERMS

unexploded ordnance (UXO), detection, discrimination, helicopter surveys

16. SECURITY CLASSIFICATION OF:			17. LIMITATION OF ABSTRACT	18. NUMBER OF PAGES	19a. NAME OF RESPONSIBLE PERSON
a. REPORT	b. ABSTRACT	c. THIS PAGE	SAR	63	Dr. Jeffrey Marqusee
Uncl.	Uncl.	Uncl.			19b. TELEPHONE NUMBER *(include area code)* 703-696-2120

Standard Form 298 (Rev. 8-98)
Prescribed by ANSI Std. Z39.18